MSc Thesis

August, 2019

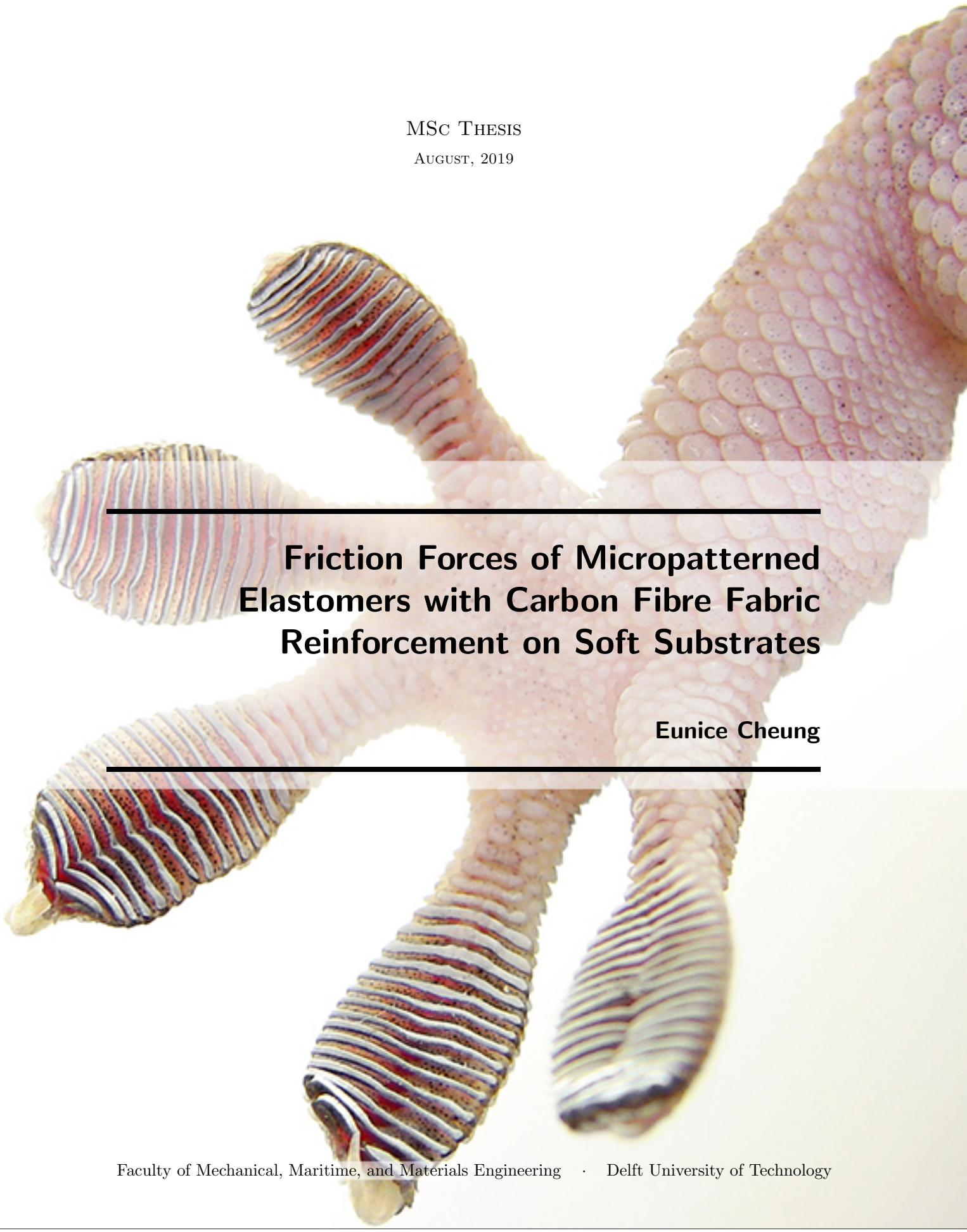

Friction Forces of Micropatterned Elastomers with Carbon Fibre Fabric Reinforcement on Soft Substrates

Eunice Cheung

Faculty of Mechanical, Maritime, and Materials Engineering · Delft University of Technology

Friction Forces of Micropatterned Elastomers with Carbon Fibre Fabric Reinforcement on Soft Substrates

Master of Science Thesis

For obtaining the degree of Master of Science in Biomedical Engineering at Delft University of Technology

Eunice Cheung

August 22, 2019

Faculty of Mechanical, Maritime, and Materials Engineering · Delft University of Technology

Picture on front page modified from https://www.flickr.com/photos/furryscalyman/3830578747.

Delft University Of Technology
Department Of
Biomechanical Engineering

The undersigned hereby certify that they have read and recommend to the Faculty of Mechanical, Maritime, and Materials Engineering for acceptance a thesis entitled **"Friction Forces of Micropatterned Elastomers with Carbon Fibre Fabric Reinforcement on Soft Substrates"** by **Eunice Cheung** in partial fulfillment of the requirements for the degree of **Master of Science**.

Dated: August 22, 2019

Dr. D. Dodou

P. van Assenbergh, M.Sc.

Dr. V. Popovich

Preface

When I started my journey as a student in Delft in September 2013, I always had in mind that, after following the curriculum of three years to obtain the BSc. in Mechanical Engineering, I would finish my studies with a MSc. degree. Little did I image my academic and personal growth of the past six years, along with my gratefulness to present my final project at Delft University of Technology.

I would firstly like to thank my supervisors, Dimitra Dodou and Peter van Assenbergh, for their guidance during this project. The hours of discussions in meetings with them provided me with insightful feedback and ideas to overcome challenges within the project. In addition, I would like to express my appreciation for the laboratory staff at the faculty of Applied Sciences for providing me with supplies to fabricate my samples.

I would like to acknowledge Henny van der Ster from the Electronic and Mechanical Support Division (DEMO) of the Delft University of Technology for his contribution to the design and fabrication of the measurement setup. Lastly, I would like to thank Vera Popovich for her time and interest to be on my committee.

Regarding my personal growth, alongside with the support of my family, I am thankful for all the circles of friends that I was lucky to meet during the past years. My friends during my exchange in Tokyo, 2015, thank you for the Sunday Morning Breakfasts, exploring a fascinating culture with me, and looking over me as I was searching for my own values. As for my moments in Delft, I am indebted to my dear friend who always manage to brighten up my day, as love goes through the stomach. I am grateful for the extraordinary people I met during my studies, who have shared enjoyable moments with me, challenged my views, and supported me during many moments of struggles with my health.

I am very content to have accepted the opportunity to study in Melbourne, 2017, even though it meant that I would be close to the last person in my circle to obtain my Master's degree. This last experience abroad completed my final goal, that I wanted to experience as a student, and left me with cherishable memories and friends with who I was able to transform dubious flats into cosy ones.

I am excited, now as a graduate, to keep striving for my goals as I continue to grow.

Eunice Cheung

Delft, August 2019

Contents

Nomenclature

Symbols

α	Significance level
A_{pad}	Surface area of adhesive pad [m^2]
df_1	Degrees of freedom
df_2	Within-groups degrees of freedom
E_{CFF}	Elastic modulus of carbon fibre fabric [Pa]
E_{eff}	Effective modulus of elasticity [Pa]
E_{pad}	Elastic modulus of adhesive pad [Pa]
E_{sub}	Elastic modulus of substrate [Pa]
F	F-statistic
p	Significance value
t_{pad}	Thickness of adhesive pad [m]

Abbreviations

ANOVA	Analysis of variance
CFF	Carbon fibre fabric
PDMS	Polydimethylsiloxane
PDMS-2	Polydimethylsiloxane in 1:20 weight ratio
PDMS-5	Polydimethylsiloxane in 1:5 weight ratio
PSA	Pressure sensitive adhesive
PU	Polyurethane
TL	Terminal layer
UD	Unidirectional

Friction Forces of Micropatterned Elastomers with Carbon Fibre Fabric Reinforcement on Soft Substrates

Eunice Cheung
Delft University of Technology

Gecko-inspired adhesives mimic the external structure of geckos with micropatterned surfaces and the internal structure by fabric reinforcement in soft elastomer adhesive pads. Previous research measured the friction forces of synthetic adhesives, with either an external or internal structure, mainly on hard substrates. Much less is known about the effects on static friction forces on soft substrates of adhesives with a combined external and internal structure and with a contact area beyond a centimetre square. We fabricated 40 by 40 mm adhesive pads ($E_{pad} = 2.1 \pm 0.1$ MPa) from polydimethylsiloxane (PDMS) elastomer and tested them on two soft PDMS substrates ($E_{sub} = 2.6 \pm 0.2$ MPa and 1.0 ± 0.1 MPa). A colloidal lithographic approach was used to fabricate the external structures of the adhesive pads with microscale dimples with and without a terminal layer (TL). The internal structures were fabricated by reinforcement of the adhesive pads with carbon fibre fabric (CFF), which varied in the types of CFF weave and its orientation with respect to the substrate. We found that samples without an external structure generated lower friction on the softer substrates, whereas samples with micropatterned surface generated similar friction between the substrates, presumably due to mechanical interlocking between the external structure and soft substrates. Samples with microscale dimples without TL generated the lowest friction forces among all samples, likely due to limited initial contact with the substrates. Samples with microscale dimples with TL generated similar friction forces as samples without an external structure. Those samples with TL were not able to generate higher friction, due to their fabrication method which restricted the movement of the fibre bundles, hindering the stress redistribution along the sample during the measurements. Samples with an internal structure showed significant higher friction compared to samples without reinforcement, due to a better stress distribution along the samples, but generated similar friction forces among the types of CFF weave.

1. Introduction

The development of biomimic pressure sensitive dry adhesives have gained interest over the past few decades. Those *pressure sensitive adhesives* (PSAs) form intimate contact with the substrate, upon application of a light pressure, to create instantaneous adhesion without required curing or treatment to enable the adhesion [1, 2]. Adhesion is enabled upon the formation of intimate contact with the substrate, mainly in form of Van der Waals forces [1]. The material properties of PSAs require a low elastic modulus to create intimate contact with the substrate, while an increase stiffness is required to prevent unintentional debonding with the substrate. The challenge to combine the two contradictory requirements, a soft and stiff material, have been the point of interest in the research field of biomimetic PSAs [3].

1.1 Adhesive Mechanisms in Geckos

Biomimetic dry adhesives are inspired from a wide variety of organisms. The tokay gecko gained interest over the last few decades, due to its ability to quickly adhere and release on a variety of surfaces, despite its relatively large body weight [4]. This exceptional ability is explained by the external and internal anatomical structure of the gecko.

The external structure of a single gecko toe is a hierarchical system with nearly five hundred thousand fibrils, i.e. microscale setae which branch off to nanoscale spatulae [5]. The fibrils interacts with the substrate by Van der Waals forces to create adhesion [6, 7]. While an individual seta is made of a very stiff material β-keratin [8], due to their high aspect ratio, an

array of setae has a low *effective modulus of elasticity* (E_{eff}) [9]. The array of setae manages to create a large number of contact points, maximising their contact area, thus adhesion, with the substrate [9, 10].

Besides the external fibrillar geometry, geckos have an internal structure of macroscale scansors. Scansors are stiff lamellar flaps and are created by the connection of stiff tendons from the skin to the skeleton of the gecko [8, 11]. Branches of tendons inserts each scansor, throughout its width, medially and laterally, providing control over each scansor [8]. The scansors contribute to the stiffness parallel to the substrate during loading, as without, the skin does not give sufficient resistance and would buckle under loading [8]. The scansors and tendons are not oriented parallel to the substrate, but attach to the skin with an angle [8, 12]. It is believed that the orientation of the scansors increases stiffness in the normal direction to the substrate [13], which improves the adhesion of the gecko over a wide range of loading angles [11]. The exact 3D arrangement of these connective tissues is largely unknown [14].

While providing in-plane stiffness, the scansors provide rotational freedom to maintain contact and generate adhesion on macroscale rough surfaces [15, 16]. The rotational freedom is also essential for the gecko to release from the substrate by hyperextension of their toes [8]. The toe peeling puts the setae in an critical angle of 30° for their release [5], regardless of the applied force [4].

1.2 Gecko-Inspired Adhesives

The research focus in the development of biomimetic dry adhesives is largely categorised into the external structure, on decreasing the E_{eff} by designing micropatterned interface of the adhesive, and into the internal structure, on increasing the in-plane stiffness by reinforcements in the adhesive. The adhesive forces of those synthetic adhesives are measured mostly on the pull-off forces (applied load out-of-plane to the adhesive), peeling forces (applied load concentrated at one edge of the adhesive), and friction forces (applied load in-plane to the adhesive; peeling at 0°). In this paper, we focused on designing adhesives with an external and internal structure to maximise the static friction forces on substrates.

Synthetic adhesives mimic the external structure of the fibrillar geometry by the fabrication of high aspect ratio micropillars. The E_{eff} of the adhesive decreases, the compliance increases, with an increasing aspect ratio of the fibrils [17]. Initial loading on the adhesive would cause the pillars to buckle to initiate contact with the substrate [18]. The contact splitting of the pillars enables the adaptability of the adhesive to microscale rough surfaces [10, 18, 19, 20], the load to be transferred uniformly over the adhesive [18, 20], and a better defect control and resistance to contamination than *flat samples* (adhesives without micropatterns) [20, 21].

The static friction forces at the fibrillated interface can be further enhanced by connecting the neighbouring micropillars at their tips with a *terminal layer* (TL). Adhesives with a TL structure are able to generate significantly higher friction than flat samples on glass substrates [19, 22, 23] and very soft substrates (E_{sub} = 120 kPa) [24]. Higher friction forces are achieved with increased interfibril spacing [19, 22, 23]. Adhesives with a TL structure generate higher friction, compared to flat adhesives, due to the crack-trapping mechanisms between the fibrils [22, 23] and additional losses of energy. The internal interfaces of the TL structure fold upon loading, which leads to a loss of elastic energy, as the micropillars and TL stretch, and frictional losses, as the interfaces slide over one other [19, 24].

The internal structure of scansors is mimicked by reinforcing soft elastomer adhesive pads with a fabric. The fabric preserves the out-of-plane rotational freedom of the elastomer to initiate contact with the substrate, but resists in-plane deformation in the direction of loading [15]. These reinforced adhesives are able to generate high friction forces, even on substrates with large scale roughness [15] and without micropatterned structures, and require a low peeling force for release [11, 15].

The purpose of the reinforcement is to maximise the compliance in the direction normal to the substrate and minimise the compliance in the direction of loading [11, 25]. Higher friction forces are, therefore, achieved by the rein-

forcement of *carbon fibre fabric* (CFF) than by other fabric materials [26], as the high stiffness of carbon fibre further maximises the in-plane stiffness of the adhesive [11, 27]. The highest friction forces are achieved with a *unidirectional* (UD) CFF weave (E_{CFF} = 33 GPa) in combination with a 5 by 5 cm *polyurethane* (PU) pad (E_{pad} = 3.1 MPa) [25]. Table A.1 shows an overview of the conducted research on adhesives with integrated fabrics measured on their peak (static) friction forces. A comparison between the friction forces among the types of CFF is not possible, as the forces are only published on the UD woven fabrics, without the mention of the forces on plain woven ones [11, 15].

The stiffness of the substrate is expected to have an influence on the friction forces of the adhesives, depending on the internal and external structure of the adhesives. Friction forces of adhesives on soft substrates could be applied in biomedical applications, such as in surgical instruments for soft-tissue manipulation. The current use of graspers during surgical procedures show a low success rate in clamping tissues to perform an action, and, as the tool depends on pinching forces, high normal forces could lead to tissue damage [28]. The development of adhesives to generate high friction forces, with minimum applied normal forces, could advance the success rates of grasping soft tissues.

Biomimicked patterned surfaces without TL generate lower friction forces on glass substrates than flat samples [24, 29, 30]. An opposite effect is observed when measuring on very soft substrates (of one order of magnitude softer than the adhesive), as the substrate deforms under loading and may conform to the external structure of the adhesive. The deformation of the substrate may lead to mechanical interlocking with the micropatterns, resulting in higher friction forces [24].

The CFF reinforced adhesives have been mainly tested on hard substrates [11, 15, 25, 26, 31]. King et al. measured friction forces of a CFF reinforced adhesive pad of 5 by 5 cm adhered to another identical CFF reinforced adhesive pad, which is a type of measurement on a soft substrate. The adhesives were made of a PU pad (E_{pad} = 3.1 MPa) reinforced with a UD CFF (E_{CFF} = 20 GPa) and generated an average force of 53 N/cm^2 over the course of 60 cycles [27].

The CFF reinforced adhesives are, compared to synthetic fibrillar adhesives, easier to manufacture, reuseable over 100 cycles without loss of force [11, 15, 27], and able to create adhesion on substrates beyond centimetre square contact areas and with large scale roughness [15]. The synthetic fibrillar adhesives are, compared to CFF reinforced adhesives, excellent in initiating intimate contact on substrates with smaller scale roughness [19], able to restore their adhesive strength over cycles after washing its surface [21], and suggested to achieve higher friction forces on soft substrates due to mechanical interlocking [24].

It is not known what the effect is on the static friction forces of adhesives with a combined external microstructure and internal CFF reinforcement, specifically measured on soft substrates with a stiffness in the same order of magnitude as the adhesive. The effect on friction of micropatterned adhesives, with a contact area beyond centimetre square, and of different CFF weaves are further investigated. Lastly, CFF reinforcement provide in-plane stiffness and rotational freedom like scansors of a gecko, but until now, CFF reinforced adhesives do not mimic the internal structure of the scansors and tendons. Friction forces of adhesives, inspired by the complex hierarchy of the scansors of geckos, with multiple attachment points and an attachment angle of the CFF (not parallel to the substrate) are further explored.

1.3 Research Goal

We investigated the static friction forces of CFF reinforced micropatterned adhesives on soft substrates, as a function of the external structure, internal structure, and the stiffness of the substrates.

Table 1 shows the overview of the samples with external and internal structure and substrate stiffness. The samples vary in the external structures categorised in flat (without micropattern), dimple (micropatterned dimples without TL), and TL (micropatterned dimples with TL). The samples in the internal structures are grouped in clear (without CFF rein-

forcement), plain (CFF reinforced), UD (CFF reinforced), and orientation (UD CFF reinforced in an angled orientation). The flat samples are the reference samples for the external structure and the clear samples for the internal structure.

The static friction forces of the samples are measured on two types of soft substrates, which stiffness is in the same order of magnitude of the adhesive. One type of substrate is softer and the other harder than the adhesive. Lastly, all samples are also measured on a glass substrate as reference.

1.4 Hypotheses

Flat samples **(1a)** would be able to initiate contact, but would lose contact easily with the soft substrates upon loading. Without an external structure, flat samples are not able to adapt to the deformation of soft substrates under loading, causing a loss of contact with the samples. The friction would be lower on the softer substrate, as this undergoes more deformation than the harder one.

Micropatterned samples **(1b)** have a lower E_{eff} than flat samples, which would increase the adaptability of the samples to soft substrates [20]. The softer substrate, which undergoes more deformation under loading, would enhance the mechanical interlocking at the micropatterned interface [24], resulting in even higher friction than on the harder substrate. It would depend on whether the substrate is soft enough for the dimple samples to generate significant mechanical interlocking to outperform the friction forces of flat samples.

TL samples **(1c)** would have the advantage to initiate contact, like flat samples [23] by their TL layer, and to possibly create mechanical interlocking with the softer substrate, as the substrates can protrude into the subsurface dimples of the TL structure [24]. In addition, the TL structure would contribute to an additional loss of elastic and friction energy [19, 24], resulting in the highest friction forces among the external structures.

Clear samples **(2a)** would be able to initiate contract with the substrates, but would not be able to achieve uniform stress distribution due to the absence of an internal structure [32]. The internal structure is of greater importance with increasing sample sizes of contact areas beyond a centimetre square. Stress decays exponentially with distance from the point of loading [33], so without an internal structure, the stresses would build up in the adhesive close to the applied load, causing early loss of contact with the substrate or rupture of the sample. The rate of stress decay decreases with an increasing in-plane stiffness by the reinforcement of stiff fabrics [32]. As clear samples are the only sample type without an internal structure, they would generate the lowest friction among the internal structures.

Orientation samples **(2b)** would have multiple attachment points of CFF into the adhesive, which would aid with the stress distribution along the sample, resulting in higher friction forces than clear samples. Compared to the plain and UD samples, orientation samples would have a reduced in-plane stiffness and an increased out-of-plane compliance. It would depend on the balance among the stress distribution, in-plane stiffness, and out-of-plane compliance of the samples, whether orientation samples would be able to generate higher friction than the other internal structures.

UD samples **(2c)** would be able to achieve higher friction forces than plain samples, due to the different compliance of the fabric in the direction normal to the substrate. UD weave has an absence of fibres in one direction of the plane, a reduced shearing between the fibres, which improves the out-of-plane compliance of the fabric [15, 34]. The compliance of fabrics is due to the rotational freedom between the fibres, which in turn allows the adhesive to conform and maintain contact with the substrate [11].

UD samples would have more out-of-plane rotational freedom than plain samples, while maintaining similar in-plane stiffness as plain samples in the direction of the applied load. The rotational freedom would gain importance to maintain friction forces on the softer substrate, as the substrate would undergo more deformation than the harder one. The higher friction forces of UD samples would also explain why previous research have not published [11, 15] or measured [26, 31] samples

with plain woven CFF.

To summarise, on the two types of soft substrates, we hypothesized that:

1) Regarding the *external structure*:

(a) Flat samples generate higher friction on harder substrates than softer substrates.

(b) Dimple and TL samples generate higher friction on softer substrates than harder substrates.

(c) TL samples generate higher friction than flat and dimple samples on all substrates.

2) Regarding the *internal structure*:

(a) Clear samples generate lower friction forces than orientation, plain and UD samples on all substrates.

(b) Orientation samples generate higher friction than clear samples.

(c) Plain samples generate lower friction than UD samples, especially on softer substrates.

2. Experimental Section

Table 1 shows the overview of the fabricated sample types with the independent variables of the external and internal structures. We selected materials and constructed a fabrication method similar to the previously conducted research on the reinforced CFF adhesives [11, 15, 25, 26, 31]. Micropatterned structures were fabricated with a colloidal lithographic approach, as in Assenbergh et al. [24]. This approach is a fast and cost-effective method to fabricate micropatterned samples [30, 35] and enables the fabrication of sample sizes beyond centimetre square area [36].

2.1 Materials

We selected two types of CFF weaves, plain and UD, with the same filament count and volume fraction (Table B.1) and similar stiffness (plain: E_{CFF} = 240 GPa; UD: E_{CFF} = 235 GPa). The filament count and volume fraction resulted to the same filler loading content (volume ratio between CFF and elastomer pad) and the stiffness to a similar compliance [11, 15] among the samples, regardless of the CFF type.

The *polydimethylsiloxane* (PDMS) adhesive pads were made of SYLGARD® 184 Silicone Elastomer, a two-part liquid component kit, prepared in 1:10 crosslinker/pre-polymer weight ratio (E_{pad} = 2.1 ± 0.1 MPa [37]). The components were mixed manually, then degassed in a vacuum chamber till all air bubbles disappeared from the mixture.

The micropatterned adhesive pads were fabricated by casting the PDMS on a colloidal monolayer, obtained by deposition of microscale particles on an untreated microscope glass slide with a dip coating process [24]. The particles had an average of diameter of 8.7 µm (SD = 1.4 µm) and a polydispersity index of 1.10 [24]. The microscope glass slides had the dimensions of 76 by 52 mm, which, in combination of the dip coating process, limited the size of adhesive pads to a maximum of 40 by 40 mm.

2.2 Fabrication Method

We manufactured steel (CRS CR4) frames to serve as molds to hold the PDMS mixture and CFF in place during the curing of the adhesive pads. Figure 1 shows the frames (left) which are assembled with nuts/bolt into a sandwich structure (right).

The step-by-step fabrication of the samples (Figure B.2) started with the base plate, a release layer (PU transparent film), then a CFF (plain or UD) placed on top of each other. The PDMS mold was positioned over the CFF and, after the CFF was flattened and the fibre directions were positioned parallel/normal to the edges of the frames, the mold was fixed with bolts/nuts. The PDMS mixture was poured into the mold, followed by degassing in the vacuum chamber till all air bubbles left the mixture. Lastly, the mixture was sealed off with another PU film and topped off with the base plate. The combination of the PU films and the pressure exerted from the bolts/nuts ensured a consistent thickness and smooth finish of the adhesive pads, as excess PDMS mixture was squeezed out of the frames. The adhesive pad acquired consistently the same dimensions as

Table 1: An overview of the tested conditions on the dependent variable of the peak friction forces. The independent variables are the external and internal structure of the samples (pictures in Figure B.1) and the substrates. The number within brackets show the number of fabricated samples or substrates. The constants are given regarding the sample and measurement method.

Samples

Sample type	External	Internal
Flat clear (6)	Flat	None
Flat plain (6)		Plain
Flat UD (5)		UD
Flat orientation (3)		UD in angle
Dimple clear (1)	Dimples	None
Dimple plain (1)		Plain
Dimple UD (1)		UD
TL plain (1)	TL	Plain

X

Substrates

Substrate type	E_{sub} (MPa)
Glass	-
PDMS-5 (5)	2.6 ± 0.2 [37]
PDMS-2 (5)	1.0 ± 0.1 [37]

Constants

Sample	Measurement
One-sided pad	200 g preload
CFF tail of 6.5 cm	200 mm/min
$A_{pad} = 160$ mm^2	Regular cleaning
$t_{pad} = 0.5$ mm	
$E_{pad} = 2.1 \pm 0.1$ MPa [37]	

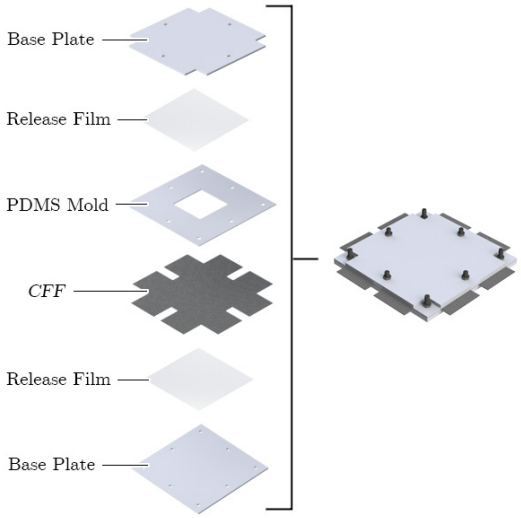

Figure 1: Frames used for the fabrication of the samples.

the PDMS mold of 40 by 40 mm ($A_{pad} = 160$ mm^2) with a thickness (t_{pad}) of 0.5 mm.

The PU film was used as release film for the fabrication of flat clear, flat plain, and flat UD samples. The top release film was replaced by a microscope glass slide with a colloidal monolayer, as mentioned before, for the fabrication of micropatterned samples. Flat orientation samples required an additional frame (Figure B.3), placed over the PDMS mold, which allowed the CFF to be inserted at an angle in the PDMS mixture (Figure B.4). The orientation of the CFF is at $52.75 \pm 2.25°$ with respect to the surface of the adhesive pad. A minimum angle is chosen which could be realised in terms of fabrication, while avoiding the critical angle of detachment of 30° in gecko's toes [4].

After the assembly of the frames, flat samples were cured for 3 hours and micropatterned samples for 24 hours at room temperature. Then all samples are cured in the oven for 24 hours at 68°C. The curing time at room temperature allows the PDMS mixture (in liquid state) to flow through the CFF and colloidal monolayer before curing at 68°C [24].

The frames were removed after curing. The CFF of the samples were cut close around the three sides of the adhesive pad, leaving a CFF tail of 45 mm wide and 65 mm long on one side of the pad. Micropatterned samples still had the microparticles embedded in the adhesive pad, so the samples were subsequently treated to dissolve those particles chemically by washing them in *N*-methyl-2-pyrrolidone [24].

TL samples were finalised in this manner: the cross-section of adhesive pad showed spher-

ical voids separated by hourglass-shaped walls; the top view showed an array of holes as the voids penetrate the TL. Dimple samples were finalised by removing the TL through covalently binding the adhesive pad on glass, after plasma cleaning of both surfaces, and subsequently peeling the sample, leaving the TL on the glass. The top view showed an avarage dimple diameter of 8.1 μm (SD = 1.17 μm, n = 100) [24].

2.3 Measurement Method

Friction forces of the samples were measured with a Lloyd Instruments LR5K material testing machine with the Lloyd Instruments XLC Series Load Cells with a 5 kN capacity for glass substrates and 100 N capacity for soft substrates. The load cell was connected to the NEXYGEN Materials Testing Software program by Lloyd Instruments. Figure 2 illustrates the measurement setup, which highlights (left) the connection of the sample to the load cell and (right) the substrate holder with the preload method.

The sample was clamped between two plates, then anchored on the load cell by a sample holder (Figure B.6) with one degree of rotational freedom in-plane with the sample by a bolt [25]. The substrate holder for the glass and soft substrates (Figure B.7) was mounted perpendicular to the base of the machine and aligned underneath the sample. The soft substrates were made in PDMS 1:5 and 1:20 weight ratio, referred respectively as PDMS-5 (E_{sub} = 2.6 ± 0.2 MPa [37]) and PDMS-2 (E_{sub} = 1.0±0.1 MPa [37]). The PDMS-5 and PDMS-2 substrates were each fabricated 5 times with an approximate thickness of 2 mm.

The friction forces of the samples on the substrates were measured at a displacement speed of 200 mm/min. The measurement were conducted in three series, each series for one of the substrates, starting with the PDMS-2, then the PDMS-5, and ending with the glass substrates. The series involved 10 measurements per sample type and the measurement sequence was randomised within each series.

Before the start of each measurement, the adhesive pad of the sample was rinsed with ethanol, cleaned with Scotch tape, then preloaded with 200 g (Figure B.8) by a manual rolling motion (5 times up-and-down) on the substrate. Every 4 measurements, the substrate was cleaned with Scotch tape. Every 16 measurements, a new PDMS substrate was used, while the same glass substrate was used during the whole measurement series. All substrates were cleaned with ethanol and Scotch tape every 16 measurements.

The consistent cleaning of the samples and substrates with ethanol and Scotch tape reduces the contamination of fingerprints and dust on the interface between the sample and substrate [38, 39]. Contamination could interfere with initiating intimate contact between the sample and substrate, which affects the measured friction forces.

2.4 Data Analysis

The raw data of the friction force measurements were processed and analysed with MATLAB R2017a (scripts found in Appendix C.4). The measurements were firstly examined with force-displacement plots to validate the usability of each measurement: a maximum peak force (the static friction) should be observed before the first loss of contact between the sample and substrate, followed by a sharp drop in forces upon loss of contact. The peak forces are subsequently extracted from each measurement.

The peak friction forces between the independent variables of external structure, internal structure, and substrate were compared with analysis of variance (ANOVA). The significance level (α) is set at 0.05. One-way ANOVAs were conducted separately on the external structures, internal structures, and substrates to have an initial understanding of the peak forces.

Analysis on the interactions between the independent variables were constrained, due to the missing samples combination among the external and internal structures (i.e. the dimple and TL orientation, TL clear, and TL UD samples were non-existent). Two-way ANOVAs were therefore conducted separately between the external structures and substrates, then between the internal structures and substrates.

3. Results

We observed the behaviour of each sample type

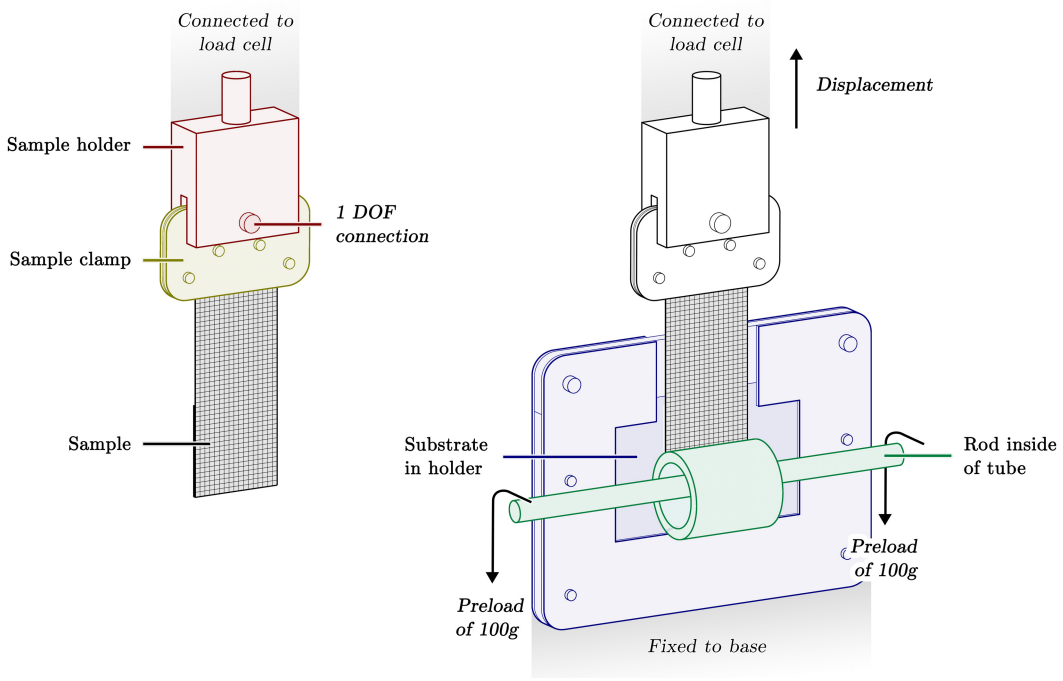

Figure 2: The measurement setup with (left) the connection of the sample to the load cell and (right) the substrate fixed perpendicularly to the base. After the preload of 200 g, the forces were measured with the displacement of the load cell. Picture of the actual measurement setup can be found in Figure B.5.

during a total of 240 measurements (8 sample types, each type measured 10 times on 3 different substrates). The duration of each measurement was only several seconds. The main results on the peak friction forces with the one- and two-way ANOVA (Table 2 – 5) are represented in the degrees of freedom (df_1), the within-groups degrees of freedom (df_2), the F-statistic (F), and significance value (p) with $\alpha = 0.05$. The levels (what is compared) are shown in *italic*, significant values in **green and bold**, and insignificant values in red. Additional tables on the results of the ANOVA are exported and found in Appendix C.3.

3.1 Video Recordings of Measurements

During the measurement, we observed that the CFF tail gets in tension, followed by peeling of the sample from the bottom, top, or sides. The sample occasionally rotated slightly in-plane with the substrate during peeling, which rotation was allowed by the sample clamp. The maximum peak force (the static friction force) was measured before the first release of the sample from the substrate.

Videos of the measurements, with a frame rate of 50 fps, captured the failure method of each sample type. It was noticeable that the sample did not create full contact with the glass substrate after preloading, as some air bubbles remained at the interface between the sample and substrate. The videos showed that the behaviour of the samples are similar across the external structure types; only that the micropatterned samples showed a less apparent behaviour than flat samples.

Plain, UD, and TL samples started peeling from the edges of the sample towards the CFF tail. Figure 3 shows the measurement of the TL sample on glass substrate and the force-time plots with the corresponding screenshots of the video.

Clear samples stretched significantly at the adhesive pad close to the CFF tail and peeled off from the tail towards the other edges of the sample. Flat clear samples on the glass substrates fractured close to the CFF tail, as the adhesive pad remained on the substrate (Fig-

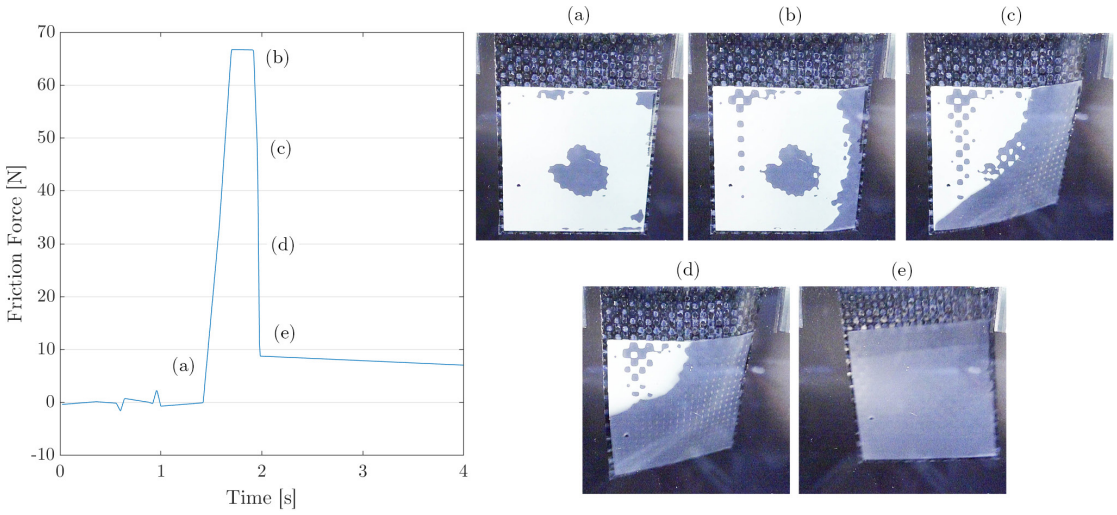

Figure 3: TL plain sample measured on the glass substrate with the friction-time plot (left) and the pictures of the sample (right) during the measurement. The behaviour of this sample was comparable with flat plain, flat UD, dimple plain, and dimple UD samples: the (a) initial position of the sample with some regions without contact (dark spots) at the interface between the sample and substrate, the CFF in full tension right before (b) the right edge of the adhesive pad starts peeling and some air bubbles grow in size, as the (c, d) peeling continues, the forces drop, and the measurement ends (e) when the sample fully loses its contact with the substrate.

ure C.1). The measured peak friction forces upon rupture were 61.04 N, 69.34 N, and 38.75 N; those measurement were not included in further data analysis. Flat orientation samples behaved in a similar manner as the clear samples, other than the stretching and peeling of the pad started at the CFF located at the middle of the adhesive pad (Figure C.2).

3.2 Effects of Combined External and Internal Structures on Soft Substrates

The peak friction forces on the PDMS-5 and PDMS-2 substrates were extracted and represented in Figure 4 (similar boxplot found in Figure C.3). Ten separate one-way ANOVAs were conducted on the external and internal structures with the PDMS-5 and PDMS-2 substrates (Table 2).

The external structures were compared among the clear (*flat clear* and *dimple clear*), plain (*flat plain*, *dimple plain*, and *TL plain*), and UD (*flat UD* and *dimple UD*) samples on each PDMS-5 and PDMS-2. Significant main effects were shown on both substrates for the clear (PDMS-5: $F(1,18) = 87.7$, $p < 0.001$; PDMS-2: $F(1,18) = 246.8$, $p < 0.001$), plain (PDMS-5: $F(2,27) = 191.5$, $p < 0.001$; PDMS-2: $F(2,27) = 499.9$, $p < 0.001$), and UD structures (PDMS-5: $F(1,18) = 140.1$, $p < 0.001$; PDMS-2: $F(1,18) = 149.7$, $p < 0.001$).

The internal structures were compared among the flat (*flat clear*, *flat plain*, *flat UD*, and *flat orientation*) and dimple (*dimple clear*, *dimple plain*, and *dimple UD*) samples on each PDMS-5 and PDMS-2. Significant main effects were shown on both substrates for the flat (PDMS-5: $F(3,36) = 78.9$, $p < 0.001$; PDMS-2: $F(3,36) = 95.6$, $p < 0.001$) and dimple structures (PDMS-5: $F(2,27) = 12.4$, $p < 0.001$; PDMS-2: $F(2,27) = 17.7$, $p < 0.001$).

Post-hoc analysis showed that, *among* plain samples, *within* each of the substrates, dimple samples generated significant lower friction than flat and TL samples ($p < 0.001$). There was no statistically significant difference in friction between flat and TL sample (PDMS-5: $p = 0.096$, PDMS-2: $p = 0.709$).

Among flat samples, the friction between flat plain and flat UD samples was not statistically significantly different (PDMS-5: $p = 0.527$, PDMS-2: $p = 1.000$). All other interactions between flat clear, flat plain, flat

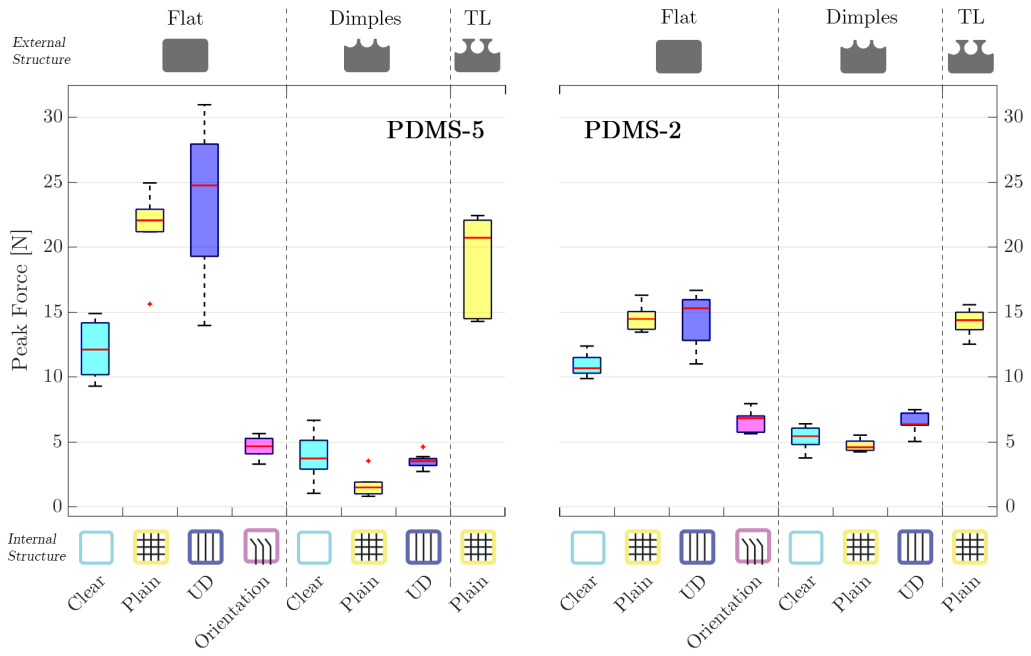

Figure 4: Peak friction forces of all samples, on PDMS-5 (left) and PDMS-2 (right) substrates, categorised in the external structure (flat, dimples, and TL) and the internal structure (clear, plain, UD, and orientation).

Table 2: One-way ANOVA for the external and internal structures were analysed separately on each substrate (PDMS-5 and PDMS-2). The levels, the samples which are compared among each group, are shown in *italic*.

				PDMS-5		**PDMS-2**	
Group	***Levels***	df_1	df_2	F	p	F	p
Clear	*Flat clear* *Dimple clear*	1	18	87.7	0.000	246.8	0.000
Plain	*Flat plain* *Dimple plain* *TL plain*	2	27	191.5	0.000	499.9	0.000
UD	*Flat UD* *Dimple UD*	1	18	140.1	0.000	149.7	0.000
Flat	*Flat clear* *Flat plain* *Flat UD* *Flat orientation*	3	36	78.9	0.000	95.6	0.000
Dimple	*Dimple clear* *Dimple plain* *Dimple UD*	2	27	12.4	0.000	17.7	0.000

UD, and flat orientation samples *within* each of the substrates were statistically significant ($p < 0.001$). Flat orientation samples generated the lowest friction, followed by flat clear samples, and lastly with the highest friction of flat plain and flat UD samples.

Among dimple samples, dimple clear samples were not significantly different from dimples UD samples on PDMS-5 ($p = 0.690$) and dimple plain samples on PDMS-2 ($p = 0.136$). The dimple plain samples generated lower friction than the dimples UD samples on PDMS-5 ($p = 0.002$) and PDMS-2 ($p < 0.001$).

3.3 Effects of Separate External and Internal Structures on Soft Substrates

Two-way ANOVAs were conducted to compare the external and internal structures separately with the substrates (Table 3). Significant main effects were shown for the external structures (*flat*, *dimples*, and *TL*: $F(2, 154) = 87.6$, $p < 0.001$) and substrates (*PDMS-5* and *PDMS-2*: $F(1, 154) = 6.0$, $p = 0.015$). A significant interaction between the external and substrate was also observed ($F(2, 154) = 9.3$, $p < 0.001$).

A significant main effect was shown for the internal structures (*clear*, *plain*, *UD*, and *orientation*: $F(3, 152) = 8.6$, $p < 0.001$), but was not statistically significant for the substrates (*PDMS-5* and *PDMS-2*: $F(1, 152) = 0.8$, $p = 0.373$). The interaction between the internal structure and substrate were not statistically significant ($F(3, 152) = 1.2$, $p = 0.311$).

Post-hoc analysis on the interaction between the external structures and substrates showed that the dimple samples generate the lowest friction compared to the flat ($p < 0.001$) and TL samples ($p < 0.001$), regardless of the comparison *within* or *across* the substrates.

Within each of the substrates, there was no statistically significant difference in friction between the flat and TL samples on the substrates (PDMS-5: $p = 0.198$; PDMS-2: $p = 0.633$). *Across* the substrates, the flat samples on PDMS-5 generated no statistically significant difference with the TL samples on PDMS-2 ($p = 0.972$). The TL samples on PDMS-5 generated higher friction than the flat ($p < 0.001$) on PDMS-2.

Table 3: Two-way ANOVA for the external structures (*flat*, *dimple*, and *TL*) and internal structures (*clear*, *plain*, *UD*, and *orientation*) were analysed separately with the substrates (*PDMS-5* and *PDMS-2*).

Group	df_1	df_2	F	p
External	2	154	87.6	**0.000**
Substrate	1	154	6.0	**0.015**
External - Substrate	2	154	9.3	**0.000**
Internal	3	152	8.6	**0.000**
Substrate	1	152	0.8	0.373
Internal - Substrate	3	152	1.2	0.311

Among the external structures, only the flat samples on PDMS-5 had slightly higher friction than on PDMS-2 ($p = 0.003$). The dimple samples ($p = 0.318$) have no statistically significant different friction on both substrates; the same applies for the TL samples ($p = 0.148$).

Post-hoc analysis on the internal structure showed that the friction was not statistically significantly different between the clear and orientation samples ($p = 0.544$) and between the plain and UD samples ($p = 0.965$). The interaction among the other internal structures were significantly different ($p < 0.05$), in which the clear and orientation samples generated the lowest friction followed by the plain and UD samples.

3.4 Effects of Combined External and Internal Structures on Glass Substrates

The peak friction forces on the glass substrates as reference were extracted and represented in Figure 5. Flat clear samples were excluded from the analysis on the glass substrates.

Four separate one-way ANOVAs were conducted on the external and internal structures on the glass substrate (Table 4). The external structures were compared among the plain (*flat plain*, *dimple plain*, and *TL plain*) and UD (*flat UD* and *dimple UD*) samples. The internal structures were compared among the flat (*flat plain*, *flat UD*, and *flat orientation*) and dimple (*dimple clear*, *dimple plain*, and *dimple UD*) samples. Significant main effects were shown for the plain ($F(2, 27) = 203.5$, $p < 0.001$), UD ($F(1, 18) = 183.0$, $p < 0.001$), flat ($F(2, 27) = 132.7$, $p < 0.001$), and dimple

($F(2, 27) = 31.1$, $p < 0.001$) samples.

Post-hoc analysis showed that, friction on glass substrates was statistically significant between all samples ($p < 0.001$), except between flat plain and flat UD samples ($p = 0.302$).

One-way ANOVA was conducted for each sample type between the *glass*, *PDMS-5*, and *PDMS-2* substrates; the flat clear samples were only compared between *PDMS-5* and *PDMS-2*. The main statistics are shown in Table 5. All samples were statistically significant ($p < 0.001$), except for flat clear ($F(1, 18) = 2.5$, $p = 0.131$) and dimple clear samples ($F(2, 27) = 2.3$, $p = 0.121$). An additional boxplot with all peak friction forces (on glass, PDMS-5, and PDMS-2) categorised per sample type can be found in Appendix C.4.

Post-hoc analysis showed that all samples, except the dimple clear samples, generated significantly higher friction on the glass substrate compared to the PDMS substrates. The friction on PDMS-5 were significantly higher than on PDMS-2 for flat orientation ($p = 0.001$), dimple plain ($p = 0.039$), and dimple UD samples ($p < 0.001$). The friction of all other samples were not statistically significantly different across the PDMS substrates ($p > 0.05$).

4. Discussion

We investigated the peak friction forces of micropatterned adhesives with CFF reinforcement on soft substrates, as a function of the external structure, internal structure, and the stiffness of the substrates. We hypothesised that:

1) Regarding the *external structure*:

- (a) Flat samples generate higher friction on PDMS-5 than PDMS-2.
- (b) Dimple and TL samples generate higher friction on PDMS-2 than PDMS-5.
- (c) TL samples generate higher friction than flat and dimple samples on all substrates.

2) Regarding the *internal structure*:

- (a) Clear samples generate lower friction forces than orientation, plain and UD samples on all substrates.
- (b) Orientation samples generate higher friction than clear samples.
- (c) Plain samples generate lower friction than UD samples, especially on PDMS-2.

Flat samples **(1a)** generated, as expected, higher friction on PDMS-5 than PDMS-2. PDMS substrates undergo deformation under loading, causing flat samples to lose contract with the substrate, as the samples are not able to conform with the substrate. This indicates the importance of an external structure to enhance the adaptability of the samples, a decreased E_{eff}, to maintain contact with softer substrates.

Dimple and TL samples **(1b)** did not generate statistically significant differences in friction between the PDMS substrates. Unlike the flat samples, micropatterned samples did not generate lower friction on PDMS-2 than PDMS-5. This suggests again that an external structure, a decreased E_{eff}, influences the friction forces on softer substrates.

Micropatterned samples might not have been able to generate higher friction forces on PDMS-2 than PDMS-5, as the effects of the external structures were not fully enabled due the lack of initial contact with the substrate. An increased preload could flatten the microstructures more, the buckling of the pillars [18], which increases the contact area of the samples with the substrates [24, 40]. Another possibility is the lack of mechanical interlocking between the micropatterns and substrates. Previous research showed that dimple samples were able to generate higher friction than flat and TL samples on substrates with an order of magnitude softer than the samples [24]. In our case, PDMS-2 substrates might not have been soft enough to undergo significant deformation to enable sufficient mechanical interlocking with the samples, as some sample types did not show statistically significant differences in friction between the PDMS substrates (Table C.4).

Dimple samples with an internal structure (plain and UD) were able to generate higher friction on PDMS-2 than PDMS-5. Without CFF reinforcement, it is possible that the mechanical interlocking of the samples would appear only close to the applied load, where all

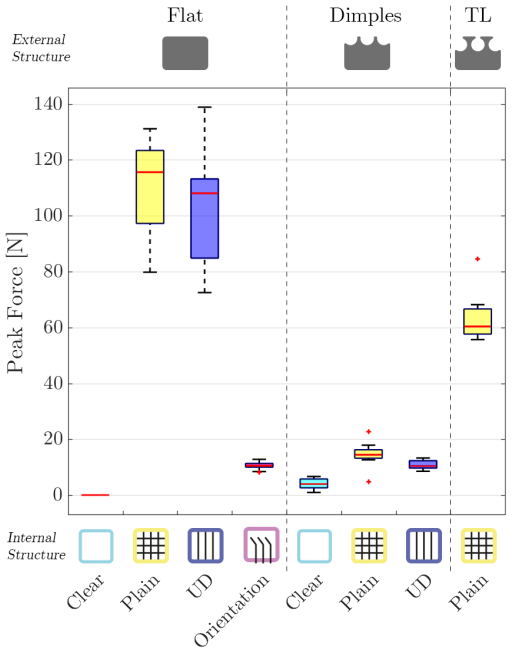

Figure 5: Peak friction forces of all samples, on glass substrates, categorised in the external structure (flat, dimples, and TL) and the internal structure (clear, plain, UD, and orientation). The data of the flat clear samples were excluded.

Table 4: One-way ANOVA for the external and internal structures on glass substrates.

Group	*Levels*	df_1	df_2	F	p
Plain	*Flat plain* *Dimple plain* *TL plain*	2	27	203.5	0.000
UD	*Flat UD* *Dimple UD*	1	18	183.0	0.000
Flat	*Flat plain* *Flat UD* *Flat orientation*	2	27	132.7	0.000
Dimple	*Dimple clear* *Dimple plain* *Dimple UD*	2	27	31.1	0.000

Table 5: One-way ANOVA for each sample type varied on *glass*, *PDMS-5*, and *PDMS-2* substrates. Flat clear samples are only compared between *PDMS-5* and *PDMS-2*.

Sample type	df_1	df_2	F	p
Flat Clear	1	18	2.5	0.131
Flat Plain	2	27	338.6	0.000
Flat UD	2	27	142.8	0.000
Flat Orientation	2	27	76.4	0.000
Dimples Clear	2	27	2.3	0.121
Dimples Plain	2	27	64.1	0.000
Dimples UD	2	27	113.6	0.000
TL Plain	2	27	249.4	0.000

stresses are concentrated. The internal structure of the dimple samples contributes to a more uniform stress distribution along the sample, due to the increased in-plane stiffness of the sample [32]. The uniform stress distribution could have enhanced the effects of mechanical interlocking of the dimples across the whole sample.

Dimple clear was the only sample that did not show any statistically significant differences in friction between all substrates (PDMS and glass substrates; see Table C.4). Moreover, there was often difficulties with the samples to initiate contact with the PDMS substrates during preloading. The reliability of the measured friction forces of dimple clear samples are therefore questionable.

TL samples **(1c)** generated comparable friction to flat samples *within* each of the substrates. Even a close comparison, including the internal structure, between the TL plain and flat plain samples had no statistical significant difference in friction between the PDMS substrates. The lack of initial contact and lack of mechanical interlocking with the substrate, as described earlier, could have caused lower friction forces of TL samples on the soft substrates. Additionally, the crack-trapping mechanisms might not be present on soft substrates, due to the conformation of the substrates [24].

More remarkably, the TL plain generated lower friction than flat plain samples on the glass substrate. It is possible that the losses of elastic and frictional energy in the TL structure are only significant for low friction forces. The losses might not scale up to the higher friction forces, especially with samples beyond centimetre contact areas. Another explanation is the behaviour of the fibre bundles, observed from the videos, in the CFF tail and in the adhesive

pad. Each (vertical) fibre bundle was pulled individually in the direction of the applied forces, starting with the bundles from the edges to the centre of the fabric. The movement and tension of the individual fibre bundles aid with the redistribution of stresses along the adhesive pad, before the sample loses contact with the substrate. This behaviour of the bundles was clearly visible for flat (plain and UD) samples, but seemed to be less pronounced for TL samples. The difference could be caused by the fabrication method, as the CFF tail of TL samples was unintentionally coated with a small layer of PDMS, during the chemical treatment to dissolve the microparticles. This layer of PDMS constrains the movement of the bundles in the direction of the forces, restricting uniform stress distribution along the sample, reducing the friction forces of TL samples.

TL samples generated, as expected, higher friction than the dimple samples. In fact, the dimple samples generated the lowest forces among the other external structures *within and across* the substrates. Even a close comparison, including the internal structure, showed that dimple plain samples generate the lowest friction compared to flat plain and TL plain samples. The poor friction forces of dimple samples underline the assumptions of the lack of initial contact and lack of mechanical interlocking with the substrate, as mentioned before.

Clear samples **(2a)** always generated a lower peak friction force than the plain or UD samples, as predicted. This underlines the importance of the internal structure, especially in adhesives beyond the centimetre square contact areas, to ensure for a proper stress distribution among adhesive pad. An evident example is the measurement of the flat clear sample on the glass substrate, which ruptured without an internal structure, close to the CFF tail where the stresses are concentrated [32].

Orientation samples **(2b)** generated comparable friction as the clear samples. Due to the fabrication method of the orientation samples, the PDMS mixture (in liquid state) crept from the adhesive pad about a centimetre into the CFF tails. The PDMS coating on the CFF tails increased the stiffness of the fabric, causing the loss of flexibility for the fabric to conform close to the adhesive pad in the direction of the applied force. The measured forces of the orientation samples were essentially peel forces in an angle of $52.75 \pm 2.25°$, instead of friction forces (peeling in $0°$).

Orientation samples were able to generate higher friction on PDMS-5 than PDMS-2. This indicates that the multiple attachment points of the CFF possibly aided with the stress distribution along the sample, causing higher friction forces on the softer substrate. An improved fabrication method of the orientation samples could potentially intensify those effects.

The friction of plain samples **(2c)** were not statistically significantly different from UD samples. A close comparison between flat plain and flat UD samples showed no significant difference in friction forces on the PDMS and glass substrates. The comparison between dimples plain and dimples UD samples did indicate that the UD CFF generates higher friction than the plain weave on the PDMS substrates.

While the UD weave has more rotational freedom than the plain weave for the sample to maintain contact with the substrate [34], the difference in friction forces might be dependent on the applied load. The rotational freedom of the CFF could likely be only significant with low measured friction forces of dimple samples. High applied loads of flat samples would put the CFF in high in-plane tension, reducing its effects of rotational freedom. Another possibility is that a high applied load would cause additional frictional energy losses in the plain CFF, that are not significant in UD CFF. Plain weave has interwoven fibres in horizontal and vertical directions in the plane, resulting in energy losses by shearing between the fibres [41].

5. Limitations and Recommendations for Future Work

Modifications on our current fabrication and measurement methods could give better understanding of the results in this work. First of all, the fabrication method of orientation samples could be further improved by increasing the number of attachment points of the fibre bundles and preventing PDMS on the CFF tail. A decreased angle of the CFF with respect to the surface of the adhesive pad, an angle less

than 30°, could further result in higher friction forces [4].

Second, the types of micropatterned samples were inadequate for the data analysis on the interaction between the external and internal structures: dimple orientation, TL orientation, TL clear, and TL UD samples were not present. Furthermore, there was only one sample per type of micropatterned sample. Improvement on the fabrication process would aid with a higher success rate for the fabrication of micropatterned sample sizes beyond centimetre square contact areas. The prevention of the PDMS coating on the CFF tail, during the chemically dissolving process of the microparticles, could also provide better insight on understanding the role of the fibre bundles on stress distribution along the samples.

Third, additional types of CFF weaves could be selected to compare the effects of the internal structure. We selected a 2/2 twill woven CFF with the same filament count and volume fraction and similar stiffness (E_{CFF} = 240 GPa) as the plain and UD woven CFF. As the twill CFF frayed too much, we excluded those samples from the measurements. Another option is to fabricate samples with CFF with an elastic modulus of an order smaller than we used for this study, a modulus similar to the CFF stiffness used in King et al. [15, 25].

Lastly, measurements with different amounts of preload can be conducted to examine whether micropatterned samples could achieve significantly higher friction forces on softer than on harder substrates. Depending on the type of micropattern and substrates, there could be a preload which results to a maximum friction force [40]. The video recordings showed that the samples were not able to achieve full contact with the substrates after preloading. An improved preload mechanism, which would consistently ensure full contact of the sample with the substrate, could result in higher friction forces.

The effect on friction forces could be explored on different stiffness of substrates, rough substrates, and wet (and soft) substrates. Larger differences in stiffness of substrates, beyond the same order of stiffness as the sample, could provide more notable contrast on the friction forces between flat and micropatterned samples. Friction forces of multiple sample types in our work did not show significant differences between the PDMS substrates (Table C.4), additionally, there was no significant statistical interaction between the internal structure and substrate. Besides the stiffness of the substrates, research can be expanded to the effects of friction forces on different macro- and microscale surface roughness of the substrates.

We fabricated soft and wet polyvinyl alcohol (PVA) substrates (E_{sub} = 18 kPa) [24], which mimic the soft and wet tissues for surgical applications of the adhesives. As the samples were not able to maintain contact with the substrates, we have not included those measurements. To measure the friction forces on PVA substrates, the samples require major structural changes to improve the adhesion with the PVA substrates. Another option is to measure the friction forces of the samples by applying a constant normal load on the samples during measurement, as in Assenbergh et al. [24].

The focus of our work has been on the variables among the external and internal structure of the samples, which excluded other essential parameters of the samples that could influence friction forces. Future research could expand on the effects of sample sizes, sample geometries, and sample stiffness on friction forces.

The chosen sample size for our experiments was determined by the maximum achievable sample size with the current fabrication method of 40 by 40 mm. Different sample sizes could result in different friction forces per unit area of the adhesive pad [15, 25]. A square sample geometry was selected for the fabrication of the adhesive pads to maximise the contact area. Previous research on CFF reinforced adhesives compared friction forces of different sample geometries with a constant contact area. Rectangular geometries with a low aspect ratio (width to length along the applied force) showed higher measured friction forces than a high aspect ratio of adhesive pads [25, 31]. Lastly, different sample stiffness could show effects on the friction forces depending on the surface roughness [15] and stiffness of the substrates [24].

6. Conclusions

We fabricated biomimetic pressure sensitive adhesives with an external micropatterned struc-

ture and internal carbon fibre fabric reinforcement. The effect on the static friction forces of the adhesives were tested on soft substrates with a stiffness in the same order of magnitude as the adhesive.

We found that flat samples (samples without external structure) generated lower friction on the softer than on the harder substrates. Similar or even higher friction forces were generated among the micropatterned samples on the softer substrate, likely due to the mechanical interlocking of the external structures to the substrate. While dimple samples generated the lowest friction among the samples, TL samples were able to generate similar friction as flat samples. The TL structure has the advantage to initiate contact with the substrate and has additional energy losses, but, presumably due to restricted movement of the fibre bundles, were not able to generate higher friction than flat samples.

The internal structure of carbon fibre fabric reinforcement resulted in significantly higher friction than samples without reinforcement. The type of fabric weave did not seem to affect the friction in samples, likely due to the decreased out-of-plane rotational freedom of the fabric upon higher applied load. Dimple samples, measured with a lower applied load, seemed to generate higher friction with an unidirectional weave than plain weave. With the current fabrication method, samples reinforced with a fabric in an angle with respect to the substrate were not able to generate significantly higher friction than samples without reinforcement.

References

[1] Benedek, I., *Pressure-sensitive adhesives and applications*, CRC Press, 2004.

[2] Pocius, A. V., *Adhesion and Adhesives Technology: an Introduction*, Hanser Gardner Publications, 2002.

[3] Heepe, L., Xue, L., and Gorb, S. N., *Bio-inspired structured adhesives: Biological prototypes, fabrication, tribological properties, contact mechanics, and novel concepts*, Vol. 9, Springer, 2017.

[4] Autumn, K., Dittmore, A., Santos, D., Spenko, M., and Cutkosky, M., "Frictional adhesion: a new angle on gecko attachment," *Journal of Experimental Biology*, Vol. 209, No. 18, 2006, pp. 3569–3579.

[5] Autumn, K., Liang, Y. A., Hsieh, S. T., Zesch, W., Chan, W. P., Kenny, T. W., Fearing, R., and Full, R. J., "Adhesive force of a single gecko foot-hair," *Nature*, Vol. 405, No. 6787, 2000, pp. 681.

[6] Autumn, K. and Peattie, A. M., "Mechanisms of adhesion in geckos," *Integrative and comparative biology*, Vol. 42, No. 6, 2002, pp. 1081–1090.

[7] Autumn, K., Sitti, M., Liang, Y. A., Peattie, A. M., Hansen, W. R., Sponberg, S., Kenny, T. W., Fearing, R., Israelachvili, J. N., and Full, R. J., "Evidence for van der Waals adhesion in gecko setae," *Proceedings of the National Academy of Sciences*, Vol. 99, No. 19, 2002, pp. 12252–12256.

[8] Russell, A. P., "A contribution to the functional analysis of the foot of the Tokay, Gekko gecko (Reptilia: Gekkonidae)," *Journal of Zoology*, Vol. 176, No. 4, 1975, pp. 437–476.

[9] Autumn, K., Majidi, C., Groff, R., Dittmore, A., and Fearing, R., "Effective elastic modulus of isolated gecko setal arrays," *Journal of Experimental Biology*, Vol. 209, No. 18, 2006, pp. 3558–3568.

[10] Varenberg, M., Murarash, B., Kligerman, Y., and Gorb, S. N., "Geometry-controlled adhesion: revisiting the contact splitting hypothesis," *Applied Physics A*, Vol. 103, No. 4, 2011, pp. 933–938.

[11] Bartlett, M. D., Croll, A. B., King, D. R., Paret, B. M., Irschick, D. J., and Crosby, A. J., "Looking Beyond Fibrillar Features to Scale Gecko-Like Adhesion," *Advanced Materials*, Vol. 24, 2012, pp. 1078–1083.

[12] Russell, A. P., "The morphological basis of weight-bearing in the scansors of the tokay gecko (Reptilia: Sauria)," *Canadian Journal of Zoology*, Vol. 64, No. 4, 1986, pp. 948–955.

[13] Tian, Y., Pesika, N., Zeng, H., Rosenberg, K., Zhao, B., McGuiggan, P., Autumn, K., and Israelachvili, J., "Adhesion and friction in gecko toe attachment and detachment," *Proceedings of the National Academy of Sciences*, Vol. 103, No. 51, 2006, pp. 19320–19325.

[14] Langowski, J. K., Schipper, H., Blij, A., van den Berg, F. T., Gussekloo, S. W., and van Leeuwen, J. L., "Force-transmitting structures in the digital pads of the tree frog Hyla cinerea: a functional interpretation," *Journal of anatomy*, Vol. 233, No. 4, 2018, pp. 478–495.

[15] King, D. R., Bartlett, M. D., Gilman, C. A., Irschick, D. J., and Crosby, A. J., "Creating Gecko-Like Adhesives for Real World Surfaces," *Advanced Materials*, Vol. 26, No. 25, 2014, pp. 4345–4351.

[16] Gillies, A. G., Henry, A., Lin, H., Ren, A., Shiuan, K., Fearing, R. S., and Full, R. J., "Gecko toe and lamellar shear adhesion on macroscopic, engineered rough surfaces," *Journal of Experimental Biology*, Vol. 217, No. 2, 2014, pp. 283–289.

[17] Glassmaker, N., Jagota, A., Hui, C.-Y., and Kim, J., "Design of biomimetic fibrillar interfaces: 1. Making contact," *Journal of the Royal Society Interface*, Vol. 1, No. 1, 2004, pp. 23–33.

[18] Jagota, A. and Bennison, S. J., "Mechanics of adhesion through a fibrillar microstructure," *Integrative and comparative biology*, Vol. 42, No. 6, 2002, pp. 1140–1145.

[19] He, Z., Hui, C.-Y., Levrard, B., Bai, Y., and Jagota, A., "Strongly modulated friction of a film-terminated ridge-channel structure," *Scientific reports*, Vol. 6, 2016, pp. 26867.

[20] Kamperman, M., Kroner, E., del Campo, A., McMeeking, R. M., and Arzt, E., "Functional Adhesive Surfaces with Gecko Effect: The Concept of Contact Splitting," *Advanced Engineering Materials*, Vol. 12, No. 5, 2010, pp. 335–348.

[21] Gorb, S., Varenberg, M., Peressadko, A., and Tuma, J., "Biomimetic mushroom-shaped fibrillar adhesive

microstructure," *Journal of The Royal Society Interface*, Vol. 4, No. 13, 2006, pp. 271–275.

[22] Vajpayee, S., Long, R., Shen, L., Jagota, A., and Hui, C.-Y., "Effect of rate on adhesion and static friction of a film-terminated fibrillar interface," *Langmuir*, Vol. 25, No. 5, 2009, pp. 2765–2771.

[23] Shen, L., Glassmaker, N. J., Jagota, A., and Hui, C.-Y., "Strongly enhanced static friction using a film-terminated fibrillar interface," *Soft Matter*, Vol. 4, No. 3, 2008, pp. 618–625.

[24] van Assenbergh, P., Fokker, M., Langowski, J., van Esch, J., Kamperman, M., and Dodou, D., "Pull-off and friction forces of micropatterned elastomers on soft substrates: the effects of pattern length scale and stiffness," *Beilstein journal of nanotechnology*, Vol. 10, No. 1, 2019, pp. 79–94.

[25] King, D. R. and Crosby, A. J., "Optimizing Adhesive Design by Understanding Compliance," *ACS applied materials & interfaces*, Vol. 7, No. 50, 2015, pp. 27771–27781.

[26] Bartlett, M. D. and Crosby, A. J., "High capacity, easy release adhesives from renewable materials," *Advanced Materials*, Vol. 26, No. 21, 2014, pp. 3405–3409.

[27] King, D. R., Bartlett, M. D., Nalbach, M., Irschick, D. J., and Crosby, A. J., "High Strength Reversible Adhesive Closures," *Journal of Polymer Science Part B: Polymer Physics*, Vol. 55, No. 23, 2017, pp. 1783–1790.

[28] Heijnsdijk, E., Dankelman, J., and Gouma, D., "Effectiveness of grasping and duration of clamping using laparoscopic graspers," *Surgical Endoscopy and other interventional Techniques*, Vol. 16, No. 9, 2002, pp. 1329–1331.

[29] Varenberg, M. and Gorb, S. N., "Hexagonal surface micropattern for dry and wet friction," *Advanced Materials*, Vol. 21, No. 4, 2009, pp. 483–486.

[30] Akerboom, S., Appel, J., Labonte, D., Federle, W., Sprakel, J., and Kamperman, M., "Enhanced adhesion of bioinspired nanopatterned elastomers via colloidal surface assembly," *Journal of The Royal Society Interface*, Vol. 12, No. 102, 2015, pp. 20141061.

[31] Bartlett, M. D., Croll, A. B., and Crosby, A. J., "Designing Bio-Inspired Adhesives for Shear Loading: From Simple Structures to Complex Patterns," *Advanced Functional Materials*, Vol. 22, 2012, pp. 4985–4992.

[32] Bartlett, M. D., *Scaling reversible adhesion in synthetic and biological systems*, Ph.D. thesis, University of Massachusetts Amherst, 2013.

[33] Kaelble, D. H., "Theory and analysis of peel adhesion: bond stresses and distributions," *Transactions of the Society of Rheology*, Vol. 4, No. 1, 1960, pp. 45–73.

[34] Edwards, K., "An overview of the technology of fibre-reinforced plastics for design purposes," *Materials & design*, Vol. 19, No. 1-2, 1998, pp. 1–10.

[35] Akerboom, S., Pujari, S. P., Turak, A., and Kamperman, M., "Controlled fabrication of polypyrrole surfaces with overhang structures by colloidal templating," *ACS applied materials & interfaces*, Vol. 7, No. 30, 2015, pp. 16507–16517.

[36] van Assenbergh, P., Meinders, E., Geraedts, J., and Dodou, D., "Nanostructure and microstructure fabrication: from desired properties to suitable processes," *Small*, Vol. 14, No. 20, 2018, pp. 1703401.

[37] Song, F. and Ren, D., "Stiffness of cross-linked poly (dimethylsiloxane) affects bacterial adhesion and antibiotic susceptibility of attached cells," *Langmuir*, Vol. 30, No. 34, 2014, pp. 10354–10362.

[38] Kroner, E., Maboudian, R., and Arzt, E., "Adhesion Characteristics of PDMS Surfaces During Repeated Pull-Off Force Measurements," *Advanced Engineering Materials*, Vol. 12, No. 5, 2010, pp. 398–404.

[39] Téllez, J. D., Sameoto, D., and Menon, C., "Cleaning properties of dry adhesives," *Science China Technological Sciences*, Vol. 53, No. 11, 2010, pp. 2942–2946.

[40] Bae, W.-G., Kim, D., and Suh, K.-Y., "Instantly switchable adhesion of bridged fibrillar adhesive via gecko-inspired detachment mechanism and its application to a transportation system," *Nanoscale*, Vol. 5, No. 23, 2013, pp. 11876–11884.

[41] Pickett, A. K., Creech, G., and de Luca, P., "Simplified and advanced simulation methods for prediction of fabric draping," *Revue Européenne des Eléments*, Vol. 14, No. 6-7, 2005, pp. 677–691.

Appendix A

Studies on Adhesives with Fabric Reinforcement

Table A.1 shows the overview of the 6 studies conducted by Bartlett and/or King [11, 15, 25, 26, 31] on adhesives with fabric reinforcement. This overview includes only the experiments which measured the friction forces on glass substrates. All information have been gathered from the published papers or supplements and are shown in the following tables on the fibre, elastomer, fabrication, and samples (Table A.2 – A.5). Unknown values are indicated with "-" and additional information are referred to the footnotes.

Table A.1: Overview of conducted research with the fibre type, polymer type, surface area of adhesive pads (A_{pad}), and peak (static) friction force per unit area of the adhesive pad (σ). Unknown values are indicated with "-", values extracted from graphs are shown in *italic*, and the highest measured σ of each study is shown in **bold**.

Ref.	Fibre Type	Polymer Type	A_{pad} (cm^2)	σ (N/cm^2)
[31]	1K Plain Weave Carbon Fibre Fabric	PDMS	- [1]	-
[11]	**12K Unidirectional Carbon Fibre Fabrics 11 oz**	**PU ST-1060**	**100** [2]	**29.5**
	Carbon Fibre/Kevlar Plain Weave 3k 4.8 oz Fabric	PDMS	-	- [3]
	Plain Weave Polyester	-	-	-
	Plain Weave Nylon Fabric	-	-	-
[26]	Fine Hemp Linen 5.3 oz	Natural Rubber Latex	100	7.1
	100% Jute Fabrics	Natural Rubber Latex	100	4.2
	Cotton Fabrics	**Natural Rubber Latex**	**100**	**8.1**
[15]	**24K Unidirectional Carbon Fibre Tape**	**PU ST1060**	**1**	***40.00***
			4	*27.50*
			9	*27.78*
			36	*22.78*
			102	*24.51*
	24K Unidirectional Carbon Fibre Tape	PU ST3040	102 [4]	*5.69* [4]
	24K Unidirectional Carbon Fibre Tape	PU F15	1 [4]	*30.00* [4]
	3K Plain Wave Carbon Fibre Fabric [5]	-	-	-
	Satin Weave S-Glass Fabric [6]	-	-	-
[25]	**24K Unidirectional Carbon Fibre Tape**	**PU ST1060**	4	*30.00*
			9	*43.33*
			16	*41.88*
			25	***76.00***
			36	*38.33*
			49	*33.47*
			64	*30.94*
			100	*24.80*
	24K Unidirectional Carbon Fibre Tape	PU F15	16 [7]	*10.63* [7]
	24K Unidirectional Carbon Fibre Tape	PU ST3040	100	-
	24K Unidirectional Carbon Fibre Tape	PU ST1075	100	-
	24K Unidirectional Carbon Fibre Tape	PU ST1085	100	-

[1] Aspect ratio of adhesive pad ranged from 0.01 to 17.5, but no friction forces are specified.
[2] A_{pad} ranged from 1 to 100 cm^2, but only the friction force for A_{pad} of 100 cm^2 is specified.
[3] Friction forces are given, but no A_{pad} specified.
[4] Highest σ shown, see Figure S3 in [15] for all friction forces for A_{pad} of 1, 4, 9, 36, and 102 cm^2.
[5] No values available, only shown in Figure 1 in [15].
[6] No values available, only shown in Video S1 in [15].
[7] Highest σ shown, see Figure 3B in [25] for all friction forces for A_{pad} of 4, 9, 16, 25, 36, 49, 64, and 100 cm^2.

Table A.2: Supplementary information on the fibre type, as the supplier information, thickness (t_{fibre}), and elastic modulus (E_{fibre}) of the fibres. Unknown values are indicated with "-" and the fibres are highlighted in **bold** in the same manner as in Table A.1.

Ref.	Fibre			
	Type	Supplier	t_{fibre} (mm)	E_{fibre} (GPa)
[31]	1K Plain Weave Carbon Fibre Fabric	Composite Envisions	-	-
[11]	**12K Unidirectional Carbon Fibre Fabrics 11 oz**	Composite Envisions	0.4	-
	Carbon Fibre/Kevlar Plain Weave 3k 4.8 oz Fabric	Composite Envisions	-	-
	Plain Weave Polyester	Jo Ann Fabrics and Crafts	-	-
	Plain Weave Nylon Fabric	Jo Ann Fabrics and Crafts	-	-
[26]	Fine Hemp Linen 5.3 oz	Hemp Traders	-	-
	100% Jute Fabrics	ATS Fabrics	-	-
	Cotton Fabrics	Jo-Ann Fabrics	-	-
[15]	**24K Unidirectional Carbon Fibre Tape**	Soller Composites	0.3	40
	3K Plain Wave Carbon Fibre Fabric	Soller Composites	-	20
	Satin Weave S-Glass Fabric	US Composites	-	10
[25]	**24K Unidirectional Carbon Fibre Tape**	Soller Composites	0.3	33

Table A.3: Supplementary information on the elastomer type, as the supplier information or other specifications, the mix ratio (if applicable), and elastic modulus (E_{pad}) of the adhesive pad. Unknown values or not applicable values are indicated with "-" and the elastomers are highlighted in **bold** in the same manner as in Table A.1.

Ref.	Elastomer			
	Type	Supplier/Specifications	Ratio	E_{pad} (MPa)
[31]	PDMS	Dow Corning Sylgrad 184	1:10	-
[11]	**PU ST-1060**	BJB Enterprises	-	3.8
	PDMS	Dow Corning Sylgrad 184	1:10	-
[26]	**Natural Rubber Latex**	Environment Technology	-	1.1
[15]	**ST1060**	BJB Enterprises	100:60	3.1
	ST3040	BJB Enterprises	100:97.5	0.3
	F15	BJB Enterprises	45:100	1.0

Table A.4: Supplementary information on the noticeable fabrication methods of the studies shown in Table A.1.

Ref.	Fabrication	
	Curing	Notes
[31]	70 deg for 14h	Mechanically cutting or attach different blocks with Sil-Poxy silicone adhesive (Smooth-On)
[11]	Room for 24h, then 70 deg for 24h; Room for 3 days (PDMS)	-
[26]	Room > 72h	Cut in size
[15]	Room > 12h, then 70 deg for 24h	Rotary blade cutter
[25]	Room > 12h, then 70 deg >12h	Rotary blade cutter

Table A.5: Supplementary information on the samples, as the dimensions, surface area of the adhesive pad (A_{pad}), the thickness of the adhesive pad (t_{pad}), peak (static) friction force (F), and the peak friction force per unit area of adhesive pad (σ). Unknown values are indicated with "-", values extracted from graphs are shown in *italic*, and the highest σ of each study is shown in **bold** in the same manner as in Table A.1.

Ref.	Samples				
	Dimensions (cm)	A_{pad} (cm^2)	t_{pad} (mm)	F (N)	σ (N/cm^2)
[31]	-	-	-	-	-
[11]	-	**100**	1	2950	**29.5**
	-	-	-	176.58	-
[26]	13.3 x 7.5	100	0.5	710	7.1
	13.3 x 7.5	100	0.5	420	4.2
	13.3 x 7.5	**100**	0.5	810	**8.1**
[15]	1 x 1	**1**	-	*40*	***40.00***
	2 x 2	4	0.42	*110*	*27.50*
	3 x 3	9	-	*250*	*27.78*
	6 x 6	36	-	*820*	*22.78*
	10.1 x 10.1	102	-	*2500*	*24.51*
	10.1 x 10.1	102	0.9	*580*	*5.69*
	1 x 1	1	0.41	*30*	*30.00*
[25]	2 x 2	4	-	*120*	*30.00*
	3 x 3	9	-	*390*	*43.33*
	4 x 4	16	-	*670*	*41.88*
	5 x 5	**25**	-	*1900*	***76.00***
	6 x 6	36	-	*1380*	*38.33*
	7 x 7	49	-	*1640*	*33.47*
	8 x 8	64	-	*1980*	*30.94*
	10 x 10	100	0.4	*2480*	*24.80*
	4 x 4	16	-	*170*	*10.63*

Appendix B

Experimental Section

B.1 Specifications of Materials

The types of CFF were selected to maintain the same filament count and volume fraction. The volume fraction was determined from the fibre area density (ρ_A) and fibre density (ρ_f). An overview of the main properties are shown in Table B.1. Table B.2 show the additional material properties with referral to the webshop or data sheets.

Table B.1: Overview of the selected CFF for the fabrication of the samples with the fibre area density (ρ_A) and fibre density (ρ_{CFF}).

Name	Weave Type	Fibre material	ρ_A (g/m^2)	Filament count (K)	ρ_{CFF} (g/cm^3)
Plain	Plain Woven	3K - 200 Tex HS	200	3	1.78
UD	Unidirectional	AKSACA A-38	200	3	1.78

Table B.2: Continuation of Table B.1 with specifications on the thickness (t_{CFF}), elastic modulus (E_{CFF}), tensile strength (σ_{CFF}), and elongation at break (ϵ_{CFF}) of the CFF.

Name	Fibre material	Tex (g/km)	t_{CFF} (mm)	E_{CFF} (GPa)	σ_{CFF} (GPa)	ϵ_{CFF} (%)
Plain[1]	3K - 200 Tex HS	200	0.32	240	3800	1.6
UD[2]	AKSACA A-38	200	0.27	235	3800	1.6

The PDMS adhesive pads and substrates were fabricated from SYLGARD® 184 Silicone Elastomer, which product information is shown the following pages.

The microscope glass slide for the fabrication of the micro-patterned samples is made of calcium soda glass with the dimensions of 76 by 52 with 1 mm thickness[3].

[1] See technical data sheet on the next page.

[2] *https://shop1.r-g.de/en/art/200157*

[3] *https://www.carlroth.com/en/en/Labware/Laboratory-Glass%2C-Vessels%2C-Consumables/Microscope-slides/Microscope-slide-in-special-size-76-x-52-mm/p/0000000f00022ec700030023_en?text=TX69.1*

TECHNICAL DATA SHEET

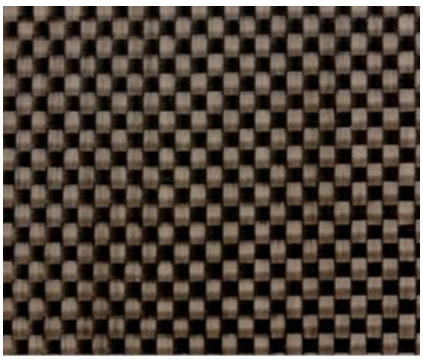

Article reference:	CAWFINPL200-100
Composition:	100% Carbon Industrial fiber
Weave:	plain
Description:	plain woven Carbon fabric balanced fabric
Surface weight:	200 g/m2 (+/- 4%)
Weave type:	plain 1/1
Fabric construction:	Warp: 5,0 ends/cm (+/- 0,1) Weft: 5,0 picks/cm (+/- 0,1)
Carbon yarn type:	Warp: 3K - Carbon: AKS HS 3K 200 Tex Weft: 3K - Carbon: AKS HS 3K 200 Tex
Fabric thickness:	0,32 mm (+/- 0,05)
Fabric width:	100 cm (+/- 1,0 cm) cut selfedges

Remarks: values as indicated by supplier.
Carbon Fiber properties: carbon fiber AKS HS 3K 200 Tex A-38 (never twisted)
Tensile strenghth: 3800 MPa - Tensile Modulus: 240 GPa
Elongation at break: 1,6% - Density 1,78 g/cm3
Sizing: 1 - 1,5 % compatible with epoxy and vinylester resin

Compositesplaza BV - Horstlandenpark 2A - 5709MB - HELMOND - the Netherlands - tel.: 0031-6-46756639 - www.compositesplaza.com

Product Information
Electronics

DOW CORNING

Sylgard® 184 Silicone Elastomer

FEATURES & BENEFITS

- Flowable
- Room temperature and heat cure
- Good dielectric properties
- Rapid, versatile cure processing controlled by temperature
- High transparency allows easy inspection of components

COMPOSITION

- Two-part
- 10 to 1 mix ratio
- Polydimethylsiloxane elastomer

Transparent encapsulant with good flame resistance

APPLICATIONS

Sylgard® 184 Silicone Elastomer is suitable for:

- LED Lighting encapsulation
- Power supplies
- Connectors
- Sensors
- Industrial controls
- Transformers
- Amplifiers
- High voltage resistor packs
- Relays
- Adhesive/encapsulant for solar cells
- Adhesive handling beam lead integrated circuits during processing

TYPICAL PROPERTIES

Specification Writers: These values are not intended for use in preparing specifications. Please contact your local Dow Corning sales office or your Global Dow Corning Connection before writing specifications on this product.

Property	Unit	Result
One or Two Part		Two
Color		Colorless
Viscosity (Base)	cP	5100
	Pa-sec	5.1
Viscosity (Mixed)	cP	3500
	Pa-sec	3.5
Thermal Conductivity	btu/hr ft ºF	0.15
	W/m ºK	0.27
Specific Gravity (Cured)		1.03
Working Time at 25ºC (Pot Life - hours)	hours	1.5
Cure Time at 25ºC	hours	48
Heat Cure Time at 100ºC	minutes	35
Heat Cure Time at 125ºC	minutes	20
Heat Cure Time at 150ºC	minutes	10
Durometer Shore		43
Dielectric Strength	volts/mil	500
	kV/mm	19

TYPICAL PROPERTIES (Continued)

Property	Unit	Result
Volume Resistivity	ohm*cm	2.9E+14
Dissipation Factor at 100 Hz		0.00257
Dissipation Factor at 100kHz		0.00133
Dielectric Constant at 100 Hz		2.72
Dielectric Constant at 100 kHz		2.68
Linear CTE (by DMA)	ppm/°C	340
Tensile Strength	PSI	980
	MPa	6.7
	Kg/cm^2	69
Refractive Index	@ 589 nm	1.4118
Refractive Index	@ 632.8 nm	1.4225
Refractive Index	@1321 nm	1.4028
Refractive Index	@ 1554 nm	1.3997
UL RTI Rating	℃	150

DESCRIPTION

Dow Corning® brand silicone 10 to 1 encapsulants are supplied as two-part liquid component kits. When liquid components are thoroughly mixed, the mixture cures to a flexible elastomer, which is well suited for the protection of electrical/electronic applications. *Dow Corning* silicone encapsulants cure without exotherm at a constant rate regardless of sectional thickness or degree of confinement.

Dow Corning® silicone elastomers require no post cure and can be placed in service immediately following the completion of the cure schedule. Standard silicone encapsulants require a surface treatment with a primer in addition to good cleaning for adhesion while primerless silicone encapsulants require only good cleaning.

APPLICATION METHODS

- Automated metered mixing and dispensing
- Manual mixing

MIXING AND DE-AIRING

The 10 to 1 mix ratio these products are supplied in gives one latitude to tune the modulus and hardness for specific application needs and production lines. In most cases de-airing is not required.

PREPARING SURFACES

In applications requiring adhesion, priming will be required for many of the silicone encapsulants. For best results, the primer should be applied in a very thin, uniform coating and then wiped off after application. After application, it should be thoroughly cured prior to application of the silicone elastomer. Additional instructions for primer usage can be found in the information sheets specific to the individual primers.

PROCESSING/CURING

Thoroughly mixed *Dow Corning* silicone encapsulant may be poured/dispensed directly into the container in which it is to be cured. Care should be taken to minimize air entrapment. When practical, pouring/dispensing should be done under vacuum, particularly if the component being potted or encapsulated has many small voids. If this technique cannot be used, the unit should be evacuated after the silicone encapsulant has been poured/dispensed. *Dow Corning* silicone encapsulants may be either room temperature (25°C/77°F) or heat cured. Room temperature cure encapsulants may also be heat accelerated for faster cure. Ideal cure conditions for each product are given in the product selection table.

POT LIFE AND CURE RATE

Cure reaction begins with the mixing process. Initially, cure is evidenced by a gradual increase in viscosity, followed by gelation and conversion to a solid elastomer. Pot life is defined as the time required for viscosity to double after base and curing agent are mixed and is highly temperature and application dependent. Please refer to the data table.

USEFUL TEMPERATURE RANGES

For most uses, silicone elastomers should be operational over a temperature range of -45 to 200°C (-49 to 392°F) for long periods of time. However, at both the low and high temperature ends of the spectrum, behavior of the materials and performance in particular

applications can become more complex and require additional considerations and should be adequately tested for the particular end-use environment. For low-temperature performance, thermal cycling to conditions such as -55°C (-67°F) may be possible, but performance should be verified for your parts or assemblies. Factors that may influence performance are configuration and stress sensitivity of components, cooling rates and hold times, and prior temperature history. At the high-temperature end, the durability of the cured silicone elastomer is time and temperature dependent. As expected, the higher the temperature, the shorter the time the material will remain useable.

COMPATIBILITY

Certain materials, chemicals, curing agents and plasticizers can inhibit the cure of addition cure gels. Most notable of these include: Organotin and other organometallic compounds, silicone rubber containing organotin catalyst, sulfur, polysulfides, polysulfones or other sulfur containing materials, unsaturated hydrocarbon plasticizers, and some solder flux residues. If a substrate or material is questionable with respect to potentially causing inhibition of cure, it is recommended that a small scale compatibility test be run to ascertain suitability in a given application. The presence of liquid or uncured product at the interface between the questionable substrate and the cured gel indicates incompatibility and inhibition of cure.

REPAIRABILITY

In the manufacture of electrical/electronic devices it is often desirable to salvage or reclaim damaged or defective units. With most non-silicone rigid potting/encapsulating materials, removal or entry is difficult or impossible without causing excessive damage to internal circuitry. *Dow Corning* silicone encapsulants can be selectively removed with relative ease, depending on the chosen remove method and technique and repairs or changes accomplished, and the repaired area repotted in place with additional product. To remove silicone elastomers, simply cut with a sharp blade or knife and tear and remove unwanted material from the area to be repaired. Sections of the adhered elastomer are best removed from substrates and circuitry by mechanical action such as scraping or rubbing and can be assisted by applying *Dow Corning*® brand OS Fluids to swell the elastomer. Before applying additional encapsulant to a repaired device, roughen the exposed surfaces of the cured encapsulant with an abrasive paper and rinse with a suitable solvent and dry. This will enhance adhesion and permit the repaired material to become an integral matrix with the existing encapsulant. Silicone prime coats are not recommended for adhering products to themselves.

PACKAGING INFORMATION

Multiple packaging sizes are available for this product. Please contact your local distributor or Dow Corning representative for information on packaging size and availability.

USABLE LIFE AND STORAGE

Shelf life is indicated by the "Use Before" date found on the product label. Refer to the product label for storage temperature requirements. Special precautions must be taken to prevent moisture from contacting these materials. Containers should be kept tightly closed and head or air space minimized. Partially filled containers should be purged with dry air or other gases, such as nitrogen.

HANDLING PRECAUTIONS

PRODUCT SAFETY INFORMATION REQUIRED FOR SAFE USE IS NOT INCLUDED IN THIS DOCUMENT. BEFORE HANDLING, READ PRODUCT AND MATERIAL SAFETY DATA SHEETS AND CONTAINER LABELS FOR SAFE USE, PHYSICAL AND HEALTH HAZARD INFORMATION. THE MATERIAL SAFETY DATA SHEET IS AVAILABLE ON THE DOW CORNING WEBSITE AT DOW CORNING.COM, OR FROM YOUR DOW CORNING SALES APPLICATION ENGINEER, OR DISTRIBUTOR, OR BY CALLING DOW CORNING CUSTOMER SERVICE.

LIMITATIONS

This product is neither tested nor represented as suitable for medical or pharmaceutical uses.

HEALTH AND ENVIRONMENTAL INFORMATION

To support customers in their product safety needs, Dow Corning has an extensive Product Stewardship organization and a team of Product Safety and Regulatory Compliance (PS&RC) specialists available in each area.

For further information, please see our website, dowcorning.com or consult your local Dow Corning representative.

LIMITED WARRANTY INFORMATION – PLEASE READ CAREFULLY

The information contained herein is offered in good faith and is believed to be accurate. However, because conditions and methods of use of our products are beyond our control, this information should not be used in substitution for customers' tests to ensure that our products are safe, effective, and fully satisfactory for the intended end use. Suggestions of use shall not be taken as inducements to infringe any patent.

Dow Corning's sole warranty is that our products will meet the sales specifications in effect at the time of shipment.

2014, April 2
Form No. 11-3184B-01

Your exclusive remedy for breach of such warranty is limited to refund of purchase price or replacement of any product shown to be other than as warranted.

DOW CORNING SPECIFICALLY DISCLAIMS ANY OTHER EXPRESS OR IMPLIED WARRANTY OF FITNESS FOR A PARTICULAR PURPOSE OR MERCHANTABILITY.

DOW CORNING DISCLAIMS LIABILITY FOR ANY INCIDENTAL OR CONSEQUENTIAL DAMAGES.

HOW CAN WE HELP YOU TODAY?

Tell us about your performance, design and manufacturing challenges. Let us put our silicon-based materials expertise, application knowledge and processing experience to work for you.

For more information about our materials and capabilities, visit **dowcorning.com**.

To discuss how we could work together to meet your specific needs, email **electronics@dowcorning.com** or go to **dowcorning.com/contactus** for a contact close to your location. Dow Corning has customer service teams, science and technology centers, application support teams, sales offices and manufacturing sites around the globe.

We help you invent the future.™

dowcorning.com

2014, April 2
Form No. 11-3184B-01

B.2 Fabrication Procedure

(a) Flat clear sample (6).

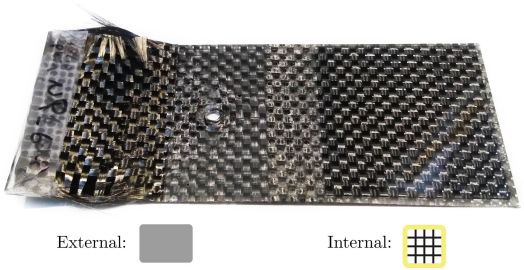

(b) Flat plain sample (6).

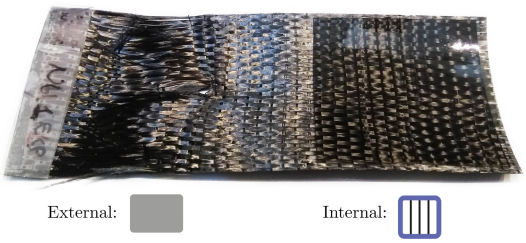

(c) Flat UD sample (5).

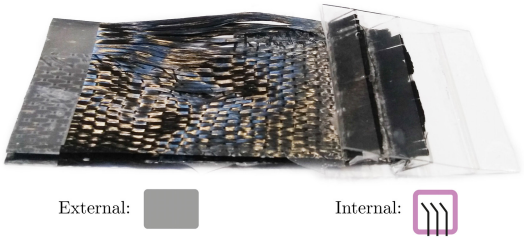

(d) Flat orientation sample (3).

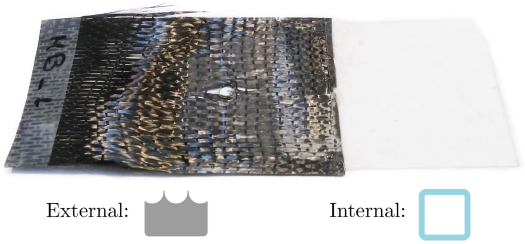

(e) Dimple clear sample (1).

(f) Dimple plain sample (1).

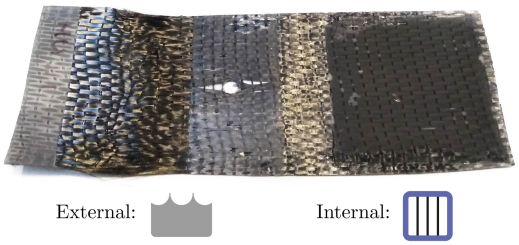

(g) Dimple UD sample (1).

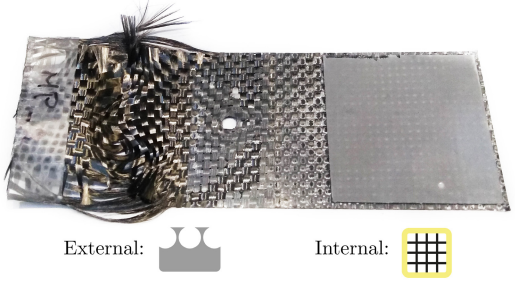

(h) TL plain sample (1).

Figure B.1: Pictures of the fabricated samples with the surface of the adhesive pad (external structure), which creates contact with the substrate, faced upwards. The illustrations of the external and internal structure of each sample is shown below the picture. The number of fabricated samples is indicated between brackets.

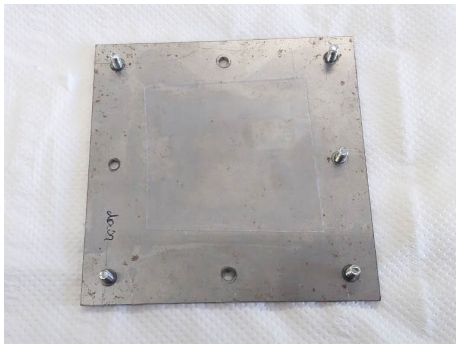

(a) The PU transparent release film is placed on the bottom base plate.

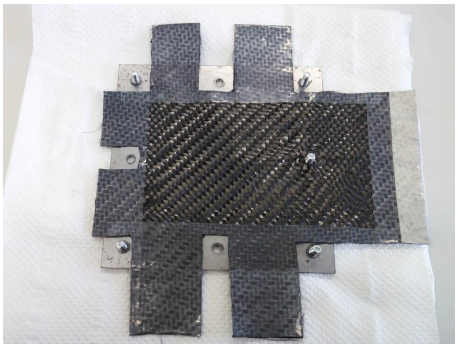

(b) The CFF is placed on the base plate with the release film.

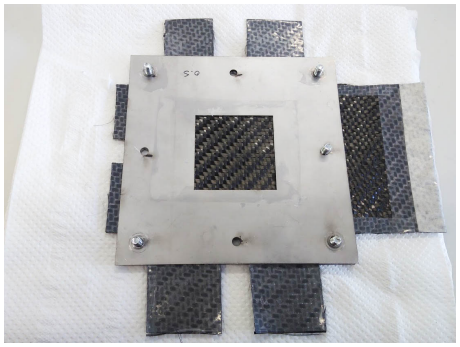

(c) The CFF is fixated in place by the PDMS mold with bolts/nuts and the PDMS mixture is poured into the mold.

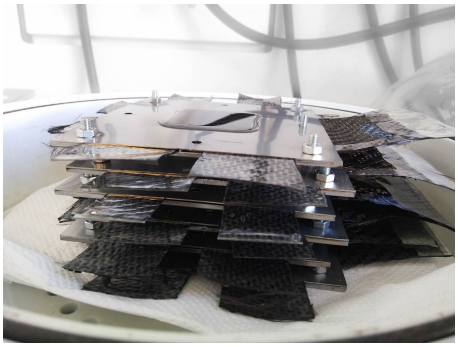

(d) The frames for multiple samples are degassed at once.

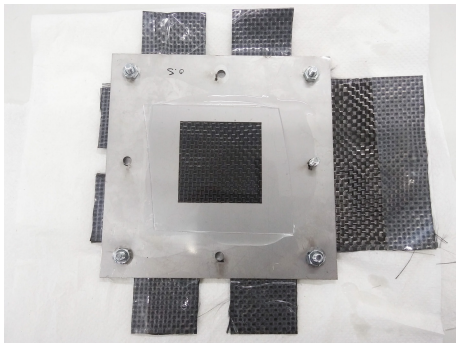

(e) The PDMS mixture is sealed with the top release film.

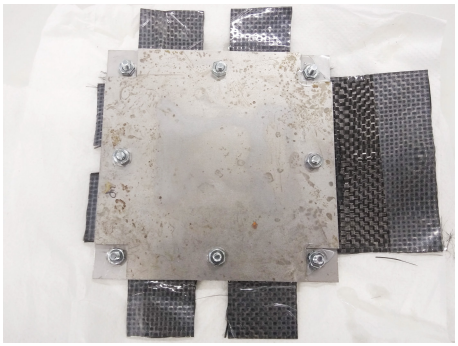

(f) The top base plate is placed and tightened with nuts.

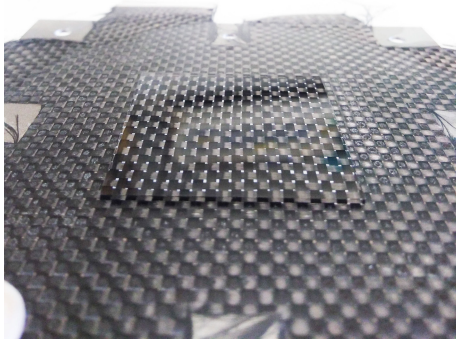

(g) Finished adhesive pad with a smooth PDMS surface.

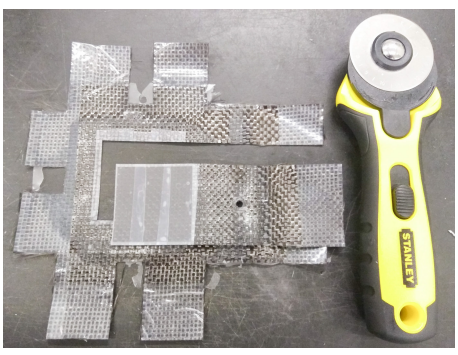

(h) The sample is cut in a CFF strip of 105 by 45 mm with a rotary blade cutter.

Figure B.2: The step-by-step fabrication process of flat clear, flat plain, and flat UD samples.

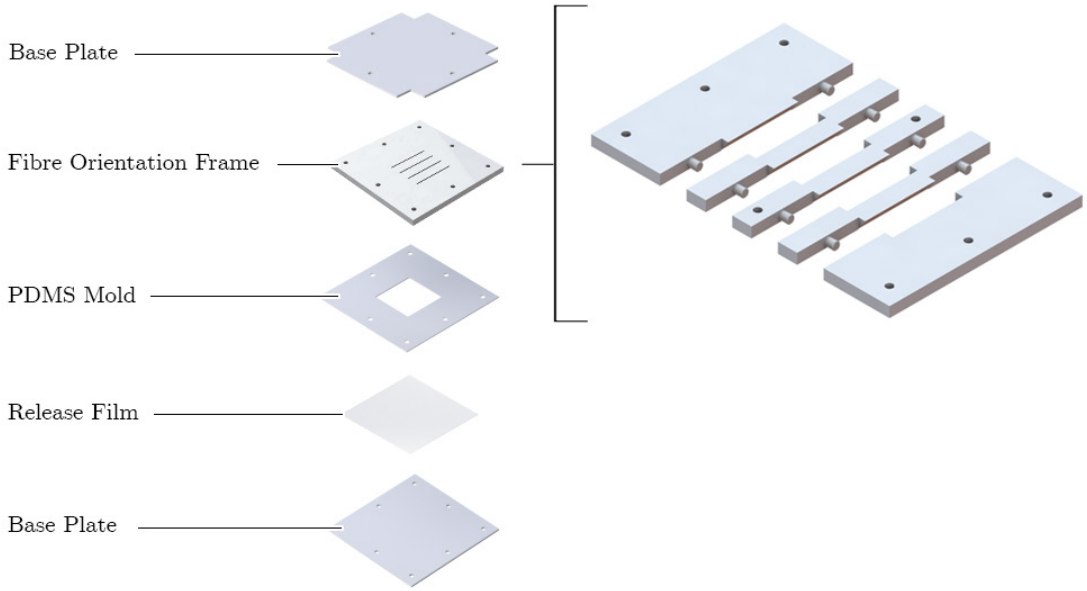

Figure B.3: Exploded view of the frames used for the fabrication of fibre orientation samples (left). The fibre orientation frame replaces the top release film in Figure 1. Exploded view of the fibre orientation frame (right) shows a 5 component frame. The components connect by the mortise and tenon joints into a frame with 4 slots for the insertion of the CFF (shown in Figure B.4). The orientation of the CFF is at $52.75 \pm 2.25^{\circ}$ with respect to the surface of the adhesive pad. The distance between each slot is 11 mm.

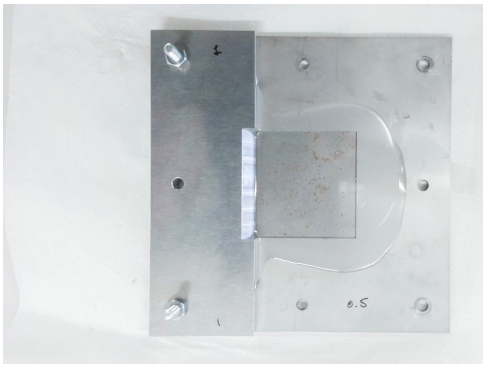

(a) The placement of first component of the fibre orientation frame on top of the base plate with release layer and PDMS mixture in the mold.

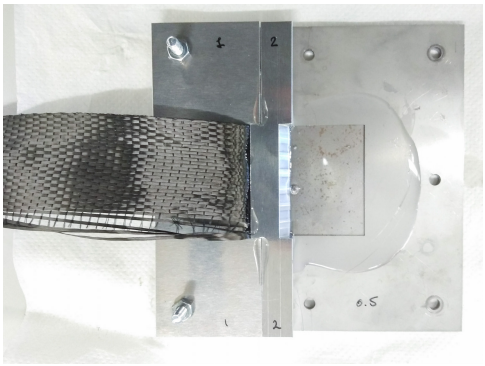

(b) The first UD CFF is submerged in the PDMS mixture, then the second component of the fibre orientation frame is placed to fixate the CFF.

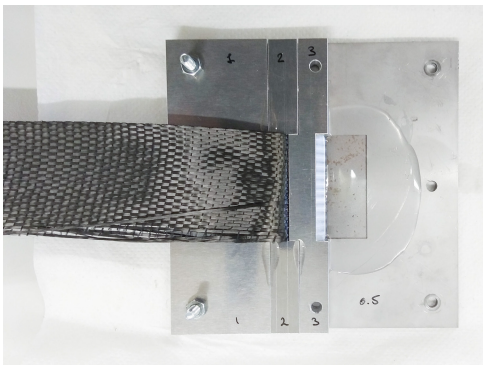

(c) The second UD CFF is submerged in the PDMS mixture, followed by the placement of the third component of the fibre orientation frame.

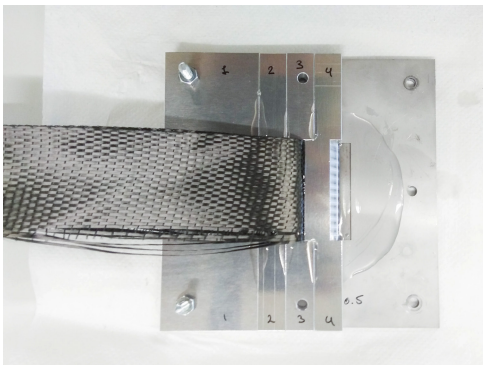

(d) Continuation of the third UD CFF and fourth component of the frame.

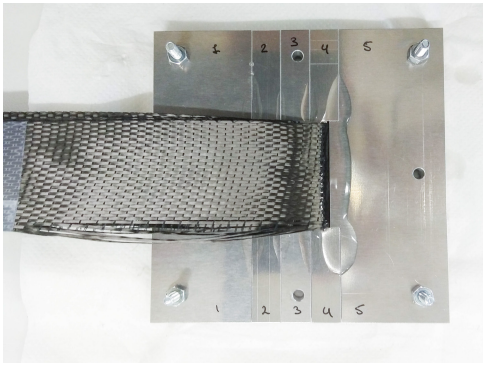

(e) Contination of the fourth UD CFF and last component of the frame.

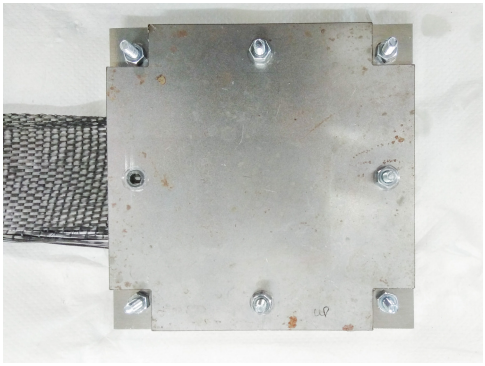

(f) The fibre orientation frame is sealed with the top base plate.

Figure B.4: The step-by-step fabrication process of flat orientation samples. UD woven CFF was used for the fabrication, due to reducing fraying of the fabric compared to the plain woven CFF. Fibre orientation samples with 4 sheets of CFF were not able to create initial contact with the substrate, as the CFF tail was not able to conform closely to the adhesive pad (as mentioned in *Discussion*). Fibre orientation samples are therefore fabricated with only 2 sheets of CFF (Figure B.1d) to increase the compliance of adhesive pad, so that the front part would be able to initiate contact with the substrate.

B.3 Measurement Setup

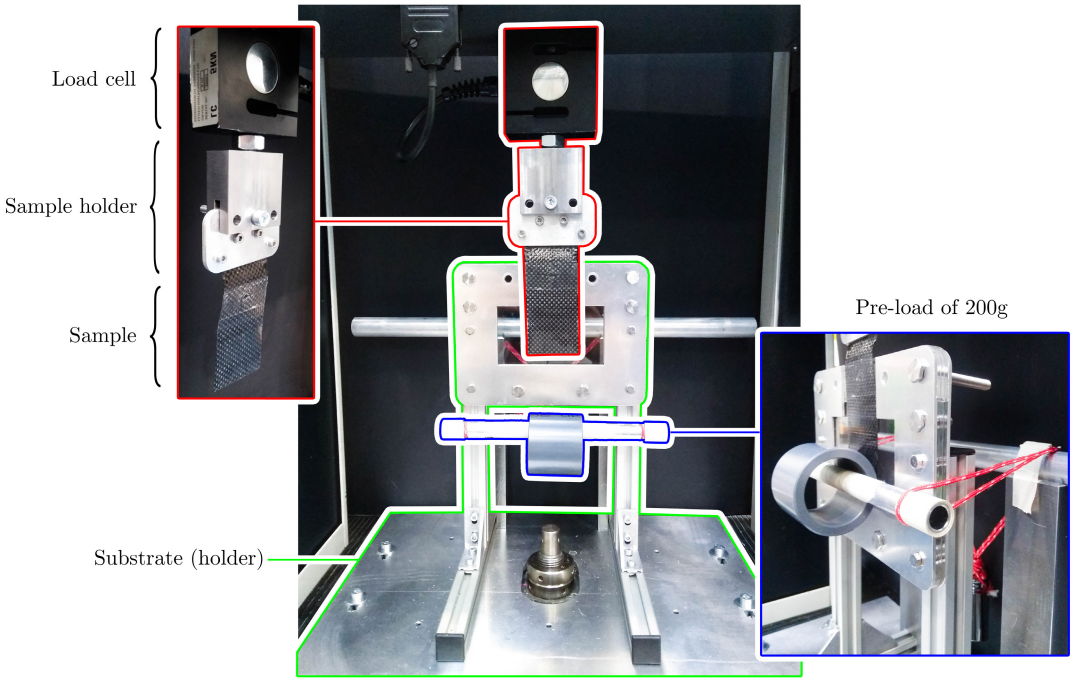

Figure B.5: Photo of the measurement setup with the sample clamping (red), substrate holder (green), and preload of 200 g (blue). An illustration of the setup is shown in Figure 2. More detailed photos of each component can be found in Figures B.6 – B.8.

(a) The CFF tail of the sample was sandwiched between two aluminium plates and fastened with 4 bolts/nuts.

(b) The sample was connected to the load cell with 5 kN capacity for the measurements with glass substrates.

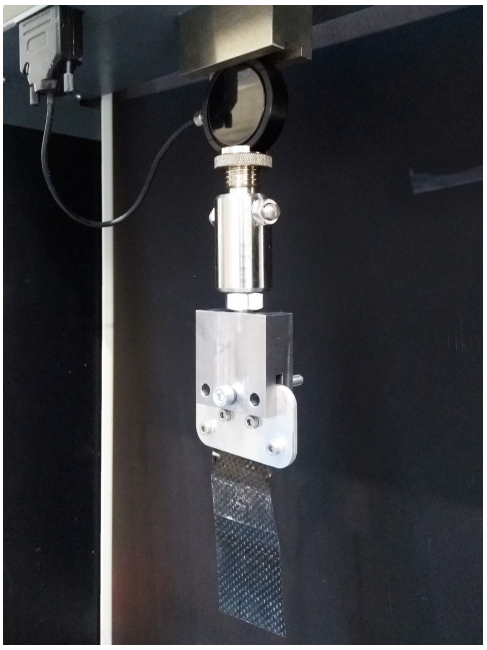

(c) The sample was connected to the load cell with 100 N capacity for the measurements with PDMS substrates.

Figure B.6: The sample clamping process, where the sample clamp was to the sample holder with 1 rotational degree of freedom in-plane with the adhesive pad.

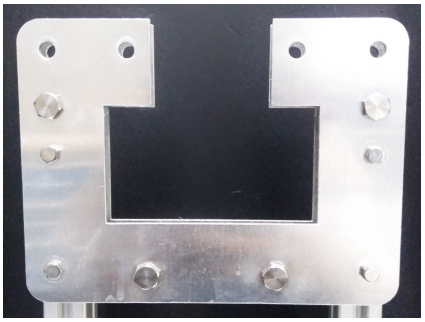

(a) Substrate holder fixated perpendicular with respect to the base plate.

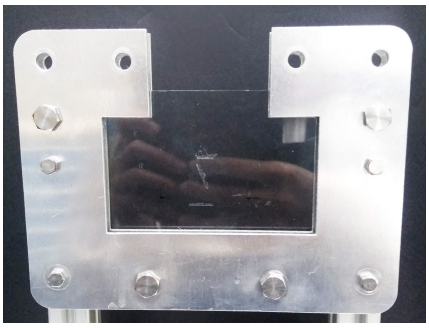

(b) The glass substrate was slit into the substrate holder.

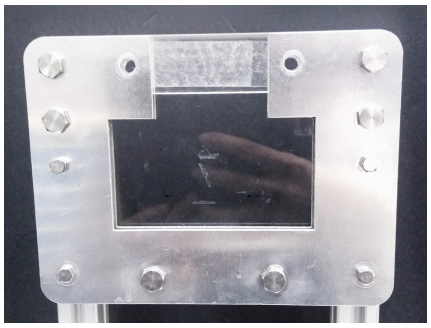

(c) The glass substrate was sealed with a top frame with bolts.

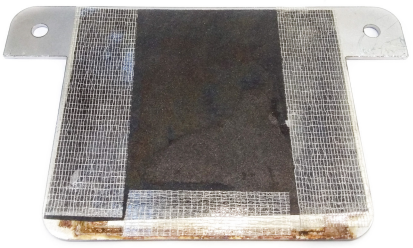

(d) The base plate for the PDMS clamping was lined with sandpaper and double sided tape to prevent slippage of the PDMS within the holder.

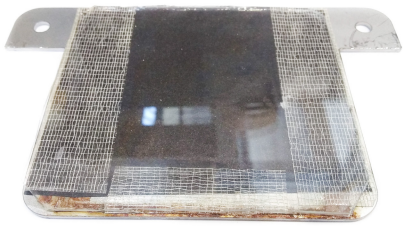

(e) The PDMS substrate was placed over the base plate.

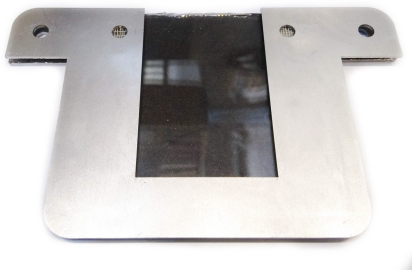

(f) The top plate, lined with double sided tape, was placed over the PDMS substrate.

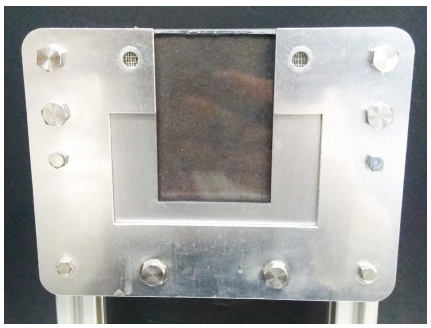

(g) The PDMS substrate was slit into the substrate holder and sealed with bolts.

Figure B.7: The clamping process of the glass (a – c) and PDMS substrates (d – g).

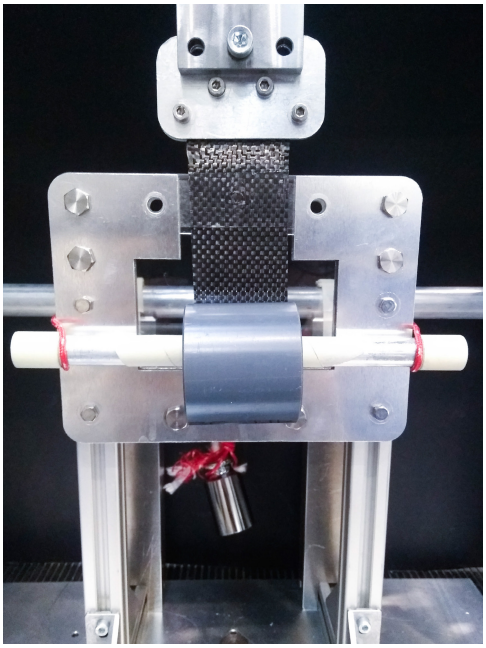

(a) The sample connected to the load cell was lowered and positioned with the substrate. The preload of 200 g was rolled 5 times over the sample.

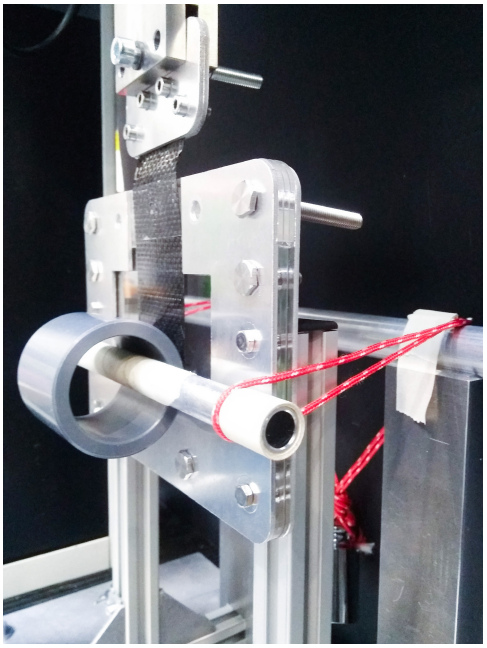

(b) The preload was carried out by a rod which was able to rotate freely inside the tube. The rod was loaded with a weight of 200 g.

Figure B.8: The preloading process of the sample onto the substrate.

Appendix C

Additional Results

C.1 Video Screenshots

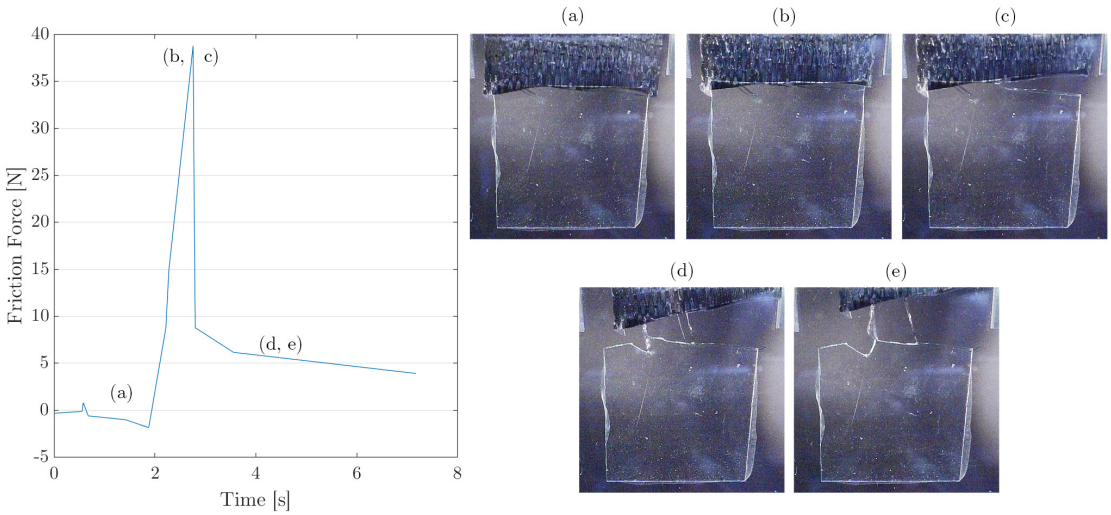

Figure C.1: Flat clear sample measured on the glass substrate with the friction-time plot (left) and the pictures of the sample (right) during the measurement: the (a) initial position of the sample, the (b) CFF tail of the sample in full tension, causing the PDMS to stretch close to the CFF tail, before the (c) rupture of the adhesive pad causing the forces to drop, and the (d, e) end of the measurement as the pad fully ruptures.

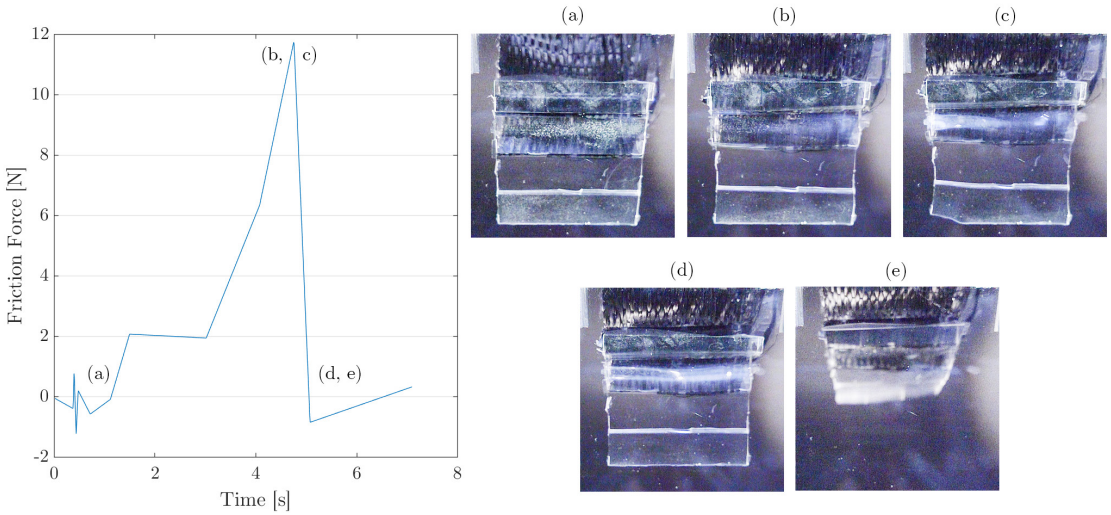

Figure C.2: Flat orientation sample measured on the glass substrate with the friction-time plot (left) and the pictures of the sample (right) during the measurement: the (a) initial position of the sample, the (b) bottom CFF tail of the sample in full tension, causing the PDMS to stretch close to the CFF tail, before the (c) peeling at the bottom of the adhesive pad causing the forces to drop, and the end of the measurement as the (d) lower half of the pad then the (e) whole pad loses contact with the substrate.

C.2 Additional Boxplots

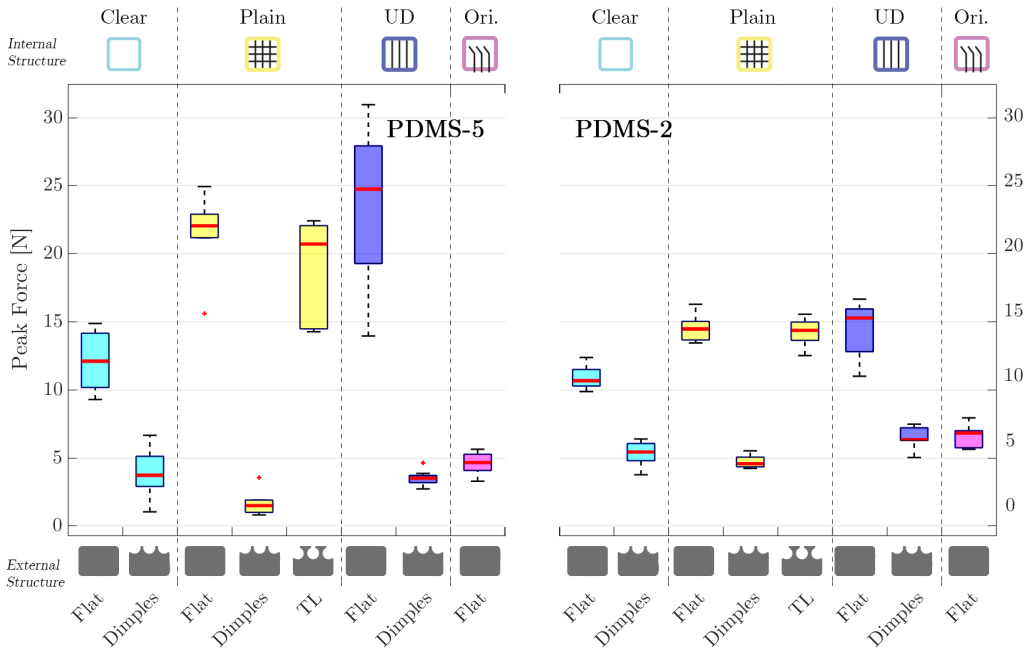

Figure C.3: Peak friction forces of all samples, on the PDMS-5 (left) and PDMS-2 (right) substrates, categorised in the internal structure (clear, plain, UD, and orientation) and the external structure (flat, dimples, and TL). This boxplot presents the same forces as in Figure 4, only categorised firstly on the internal then the external structure.

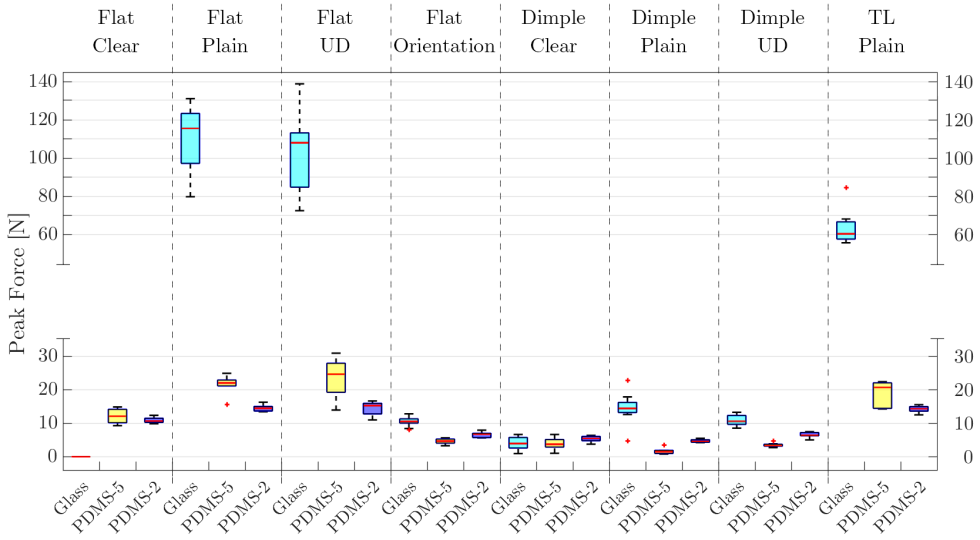

Figure C.4: Peak friction forces categorised per sample type with the glass, PDMS-5, and PDMS-2 substrates. Flat clear samples were excluded from the glass substrate measurement. The friction on the glass substrates is significantly higher than on PDMS-5 and PDMS-2 of every sample ($p < 0.001$), except for the dimple clear sample (Table 5: $F(2, 27) = 2.3$, $p = 0.121$). The friction on PDMS-5 was lower than on PDMS-2 for the fibre orientation ($p < 0.001$), dimple plain ($p = 0.039$), and dimple UD ($p < 0.001$) samples. All other samples had no statistically significant different friction ($p > 0.05$) between PDMS-5 and PDMS-2 (Table C.4).

C.3 ANOVA Data Sheets

The main results of the ANOVA are represented in the degrees of freedom (df_1), the within-groups degrees of freedom (df_2), the F-statistic (F), and significance value (p) with $\alpha = 0.05$. The post-hoc analysis show the comparison between two groups (Group 1 and Group 2) with the upper (UCI) and lower confidence interval (LCI), and significance level (p). Significant values are shown in **green and bold** and insignificant values in red.

Table C.1: One-Way ANOVA post-hoc among the plain samples for each substrate (glass, PDMS-5, and PDMS-2) with the samples: FP (flat plain), DP (dimples plain), and TP (TL plain). The main effects on the PDMS and glass substrates can be found in Table 2 and 4.

	Group 1	Group 2	LCI	Estimate	UCI	p
Glass	FP	DP	85.1	97.0	108.9	**0.000**
	FP	TP	36.5	48.4	60.4	**0.000**
	DP	TP	-60.5	-48.6	-36.7	**0.000**
PDMS-5	FP	DP	17.4	20.2	22.9	**0.000**
	FP	TP	-0.4	2.4	5.2	0.096
	DP	TP	-20.5	-17.7	-14.9	**0.000**
PDMS-2	FP	DP	8.9	9.8	10.7	**0.000**
	FP	TP	-0.6	0.3	1.2	0.709
	DP	TP	-10.4	-9.5	-8.6	**0.000**

Table C.2: One-Way ANOVA post-hoc analysis among the flat samples for each substrate (glass, PDMS-5, and PDMS-2) with the samples: FC (flat clear), FP (flat plain), FU (flat UD), and FO (flat orientation). The data on the glass substrate with the FC samples were excluded. The main effects on the PDMS and glass substrates can be found in Table 2 and 4.

	Group 1	Group 2	LCI	Estimate	UCI	p
Glass	FC	FP	-	-	-	-
	FC	FU	-	-	-	-
	FC	FO	-	-	-	-
	FP	FU	-6.6	10.3	27.2	0.302
	FP	FO	84.1	101.0	118.0	**0.000**
	FU	FO	73.8	90.7	107.7	**0.000**
PDMS-5	FC	FP	-13.6	-9.8	-6.0	**0.000**
	FC	FU	-15.5	-11.7	-7.9	**0.000**
	FC	FO	3.6	7.4	11.2	**0.000**
	FP	FU	-5.7	-1.9	1.9	0.527
	FP	FO	13.3	17.1	21.0	**0.000**
	FU	FO	15.3	19.1	22.9	**0.000**
PDMS-2	FC	FP	-5.1	-3.6	-2.2	**0.000**
	FC	FU	-5.1	-3.7	-2.2	**0.000**
	FC	FO	2.7	4.2	5.6	**0.000**
	FP	FU	-1.5	0.0	1.4	1.000
	FP	FO	6.4	7.8	9.3	**0.000**
	FU	FO	6.4	7.8	9.3	**0.000**

Table C.3: One-Way ANOVA post-hoc analysis among the dimple samples for each substrate (glass, PDMS-5, and PDMS-2) with the samples: DC (dimple clear), DP (dimple plain), and DU (dimple UD). The main effects on the PDMS and glass substrates can be found in Table 2 and 4.

	Group 1	Group 2	LCI	Estimate	UCI	p
Glass	DC	DP	-13.9	-10.5	-7.2	**0.000**
	DC	DU	-10.1	-6.8	-3.4	**0.000**
	DP	DU	0.4	3.8	7.2	**0.025**
PDMS-5	DC	DP	1.1	2.3	3.6	**0.000**
	DC	DU	-0.8	0.4	1.7	0.690
	DP	DU	-3.2	-1.9	-0.7	**0.002**
PDMS-2	DC	DP	-0.2	0.6	1.4	0.136
	DC	DU	-1.9	-1.2	-0.4	**0.002**
	DP	DU	-2.5	-1.8	-1.0	**0.000**

Table C.4: One-Way ANOVA post-hoc analysis on the substrates for each sample type: G (glass), P5 (PDMS-5), and P2 (PDMS-2). The main effects on each sample type can be found in Table 5.

Sample type	Group 1	Group 2	LCI	Estimate	UCI	p
Flat Plain	G	P5	79.5	89.8	100.1	**0.000**
	G	P2	86.8	97.1	107.4	**0.000**
	P5	P2	-3.1	7.3	17.6	0.207
Flat UD	G	P5	63.6	77.6	91.6	**0.000**
	G	P2	72.8	86.8	100.7	**0.000**
	P5	P2	-4.8	9.2	23.2	0.252
Flat Orientation	G	P5	4.7	5.9	7.1	**0.000**
	G	P2	2.6	3.9	5.1	**0.000**
	P5	P2	-3.3	-2.1	-0.9	**0.001**
Dimple Clear	G	P5	-1.7	0.1	1.9	0.991
	G	P2	-3.1	-1.3	0.5	0.194
	P5	P2	-3.2	-1.4	0.4	0.155
Dimple Plain	G	P5	10.0	13.0	15.9	**0.000**
	G	P2	6.9	9.9	12.8	**0.000**
	P5	P2	-6.1	-3.1	-0.1	**0.039**
Dimple UD	G	P5	6.1	7.3	8.5	**0.000**
	G	P2	3.1	4.3	5.5	**0.000**
	P5	P2	-4.2	-3.0	-1.8	**0.000**
TL Plain	G	P5	37.9	43.8	49.8	**0.000**
	G	P2	43.0	48.9	54.9	**0.000**
	P5	P2	-0.9	5.1	11.1	0.105

Table C.5: Two-Way ANOVA post-hoc analysis on external structures: F (flat), D (dimples), and T (TL); and on the internal structures: C (clear), P (plain), U (UD), and O (orientation). The main effects can be found in Table 3.

	Group 1	Group 2	LCI	Estimate	UCI	*p*
External	F	D	7.4	9.3	11.2	**0.000**
	F	T	-6.0	-3.2	-0.4	**0.018**
	D	T	-15.4	-12.5	-9.7	**0.000**
Internal	C	P	-8.1	-4.7	-1.2	**0.003**
	C	U	-7.8	-4.0	-0.3	**0.029**
	C	O	-2.2	2.4	7.0	0.544
	P	U	-2.8	0.6	4.0	0.965
	P	O	2.7	7.0	11.4	**0.000**
	U	O	1.8	6.4	11.0	**0.002**

Table C.6: Two-Way ANOVA post-hoc analysis on the external structures: F (flat), D (dimples), and T (TL); and substrates: P5 (PDMS-5) and P2 (PDMS-2). The main effects can be found in Table 3.

	Group 1	Group 2	LCI	Estimate	UCI	*p*
External - Substrate	F - P5	D - P5	9.3	12.5	15.7	**0.000**
	F - P5	T - P5	-8.6	-3.8	0.9	0.198
	F - P5	F - P2	0.9	3.9	6.9	**0.003**
	F - P5	D - P2	6.8	10.0	13.2	**0.000**
	F - P5	T - P2	-3.5	1.3	6.0	0.972
	D - P5	T - P5	-21.2	-16.3	-11.4	**0.000**
	D - P5	F - P2	-11.9	-8.6	-5.4	**0.000**
	D - P5	D - P2	-5.9	-2.5	1.0	0.318
	D - P5	T - P2	-16.1	-11.2	-6.3	**0.000**
	T - P5	F - P2	2.9	7.7	12.4	**0.000**
	T - P5	D - P2	8.9	13.8	18.7	**0.000**
	T - P5	T - P2	-0.9	5.1	11.1	0.148
	F - P2	D - P2	2.9	6.1	9.4	**0.000**
	F - P2	T - P2	-7.3	-2.6	2.2	0.633
	D - P2	T - P2	-13.6	-8.7	-3.8	**0.000**

C.4 MATLAB Scripts

```
%-------------------------------------------------------------------------
% IMPORT TXT-FILES AND SAVE TO MAT-FILE
%-------------------------------------------------------------------------

clear all

% importdata settings
delimiterIn = '\t';
headerlinesIn = 1;

% paths to substrates
path_G  = 'C:\Users\Eunice Cheung\Dropbox\Eunice\Thesis\Experiments\Data\Glass\';
path_P5 = 'C:\Users\Eunice Cheung\Dropbox\Eunice\Thesis\Experiments\Data\PDMS_05\';
path_P2 = 'C:\Users\Eunice Cheung\Dropbox\Eunice\Thesis\Experiments\Data\PDMS_20\';


%-----------------
% paths
%-----------------

% glass
path_G_FC = dir(strcat(path_G, 'G_NB*.txt'));
path_G_FP = dir(strcat(path_G, 'G_NP*.txt'));
path_G_FU = dir(strcat(path_G, 'G_NU*.txt'));
path_G_FO = dir(strcat(path_G, 'G_NF*.txt'));

path_G_DC = dir(strcat(path_G, 'G_MB*.txt'));
path_G_DP = dir(strcat(path_G, 'G_MP_1*.txt'));
path_G_DU = dir(strcat(path_G, 'G_MU*.txt'));

path_G_TP = dir(strcat(path_G, 'G_MP_2*.txt'));


% 1:5 PDMS
path_P5_FC = dir(strcat(path_P5, 'P05_NB*.txt'));
path_P5_FP = dir(strcat(path_P5, 'P05_NP*.txt'));
path_P5_FU = dir(strcat(path_P5, 'P05_NU*.txt'));
path_P5_FO = dir(strcat(path_P5, 'P05_NF*.txt'));

path_P5_DC = dir(strcat(path_P5, 'P05_MB*.txt'));
path_P5_DP = dir(strcat(path_P5, 'P05_MP_1*.txt'));
path_P5_DU = dir(strcat(path_P5, 'P05_MU*.txt'));

path_P5_TP = dir(strcat(path_P5, 'P05_MP_2*.txt'));


% 1:20 PDMS
path_P2_FC = dir(strcat(path_P2, 'P20_NB*.txt'));
path_P2_FP = dir(strcat(path_P2, 'P20_NP*.txt'));
path_P2_FU = dir(strcat(path_P2, 'P20_NU*.txt'));
path_P2_FO = dir(strcat(path_P2, 'P20_NF*.txt'));

path_P2_DC = dir(strcat(path_P2, 'P20_MB*.txt'));
path_P2_DP = dir(strcat(path_P2, 'P20_MP_1*.txt'));
path_P2_DU = dir(strcat(path_P2, 'P20_MU*.txt'));

path_P2_TP = dir(strcat(path_P2, 'P20_MP_2*.txt'));

% check size struct, should be (10x1)


%----------------------
% create matrices
%----------------------
```

```
65
66  for i=1:10
67      % glass
68              raw.G_FC_{i} = cell(1000,3);     % no data of G_FC
69      i_G_FP = importdata(strcat(path_G, path_G_FP(i).name),delimiterIn,headerlinesIn
        );
70              raw.G_FP_{i} = i_G_FP.data;
71      i_G_FU = importdata(strcat(path_G, path_G_FU(i).name),delimiterIn,headerlinesIn
        );
72              raw.G_FU_{i} = i_G_FU.data;
73      i_G_FO = importdata(strcat(path_G, path_G_FO(i).name),delimiterIn,headerlinesIn
        );
74              raw.G_FO_{i} = i_G_FO.data;
75
76      i_G_DC = importdata(strcat(path_G, path_G_DC(i).name),delimiterIn,headerlinesIn
        );
77              raw.G_DC_{i} = i_G_DC.data;
78      i_G_DP = importdata(strcat(path_G, path_G_DP(i).name),delimiterIn,headerlinesIn
        );
79              raw.G_DP_{i} = i_G_DP.data;
80      i_G_DU = importdata(strcat(path_G, path_G_DU(i).name),delimiterIn,headerlinesIn
        );
81              raw.G_DU_{i} = i_G_DU.data;
82
83      i_G_TP = importdata(strcat(path_G, path_G_TP(i).name),delimiterIn,headerlinesIn
        );
84              raw.G_TP_{i} = i_G_TP.data;
85
86
87      % 1:5 PDMS
88      i_P5_FC = importdata(strcat(path_P5, path_P5_FC(i).name),delimiterIn,
        headerlinesIn);
89              raw.P5_FC_{i} = i_P5_FC.data;
90      i_P5_FP = importdata(strcat(path_P5, path_P5_FP(i).name),delimiterIn,
        headerlinesIn);
91              raw.P5_FP_{i} = i_P5_FP.data;
92      i_P5_FU = importdata(strcat(path_P5, path_P5_FU(i).name),delimiterIn,
        headerlinesIn);
93              raw.P5_FU_{i} = i_P5_FU.data;
94      i_P5_FO = importdata(strcat(path_P5, path_P5_FO(i).name),delimiterIn,
        headerlinesIn);
95              raw.P5_FO_{i} = i_P5_FO.data;
96
97      i_P5_DC = importdata(strcat(path_P5, path_P5_DC(i).name),delimiterIn,
        headerlinesIn);
98              raw.P5_DC_{i} = i_P5_DC.data;
99      i_P5_DP = importdata(strcat(path_P5, path_P5_DP(i).name),delimiterIn,
        headerlinesIn);
100             raw.P5_DP_{i} = i_P5_DP.data;
101     i_P5_DU = importdata(strcat(path_P5, path_P5_DU(i).name),delimiterIn,
        headerlinesIn);
102             raw.P5_DU_{i} = i_P5_DU.data;
103
104     i_P5_TP = importdata(strcat(path_P5, path_P5_TP(i).name),delimiterIn,
        headerlinesIn);
105             raw.P5_TP_{i} = i_P5_TP.data;
106
107
108     % 1:20 PDMS
109     i_P2_FC = importdata(strcat(path_P2, path_P2_FC(i).name),delimiterIn,
        headerlinesIn);
110             raw.P2_FC_{i} = i_P2_FC.data;
111     i_P2_FP = importdata(strcat(path_P2, path_P2_FP(i).name),delimiterIn,
        headerlinesIn);
112             raw.P2_FP_{i} = i_P2_FP.data;
113     i_P2_FU = importdata(strcat(path_P2, path_P2_FU(i).name),delimiterIn,
        headerlinesIn);
```

```
114             raw.P2_FU_{i} = i_P2_FU.data;
115     i_P2_FO = importdata(strcat(path_P2, path_P2_FO(i).name),delimiterIn,
        headerlinesIn);
116             raw.P2_FO_{i} = i_P2_FO.data;
117
118     i_P2_DC = importdata(strcat(path_P2, path_P2_DC(i).name),delimiterIn,
        headerlinesIn);
119             raw.P2_DC_{i} = i_P2_DC.data;
120     i_P2_DP = importdata(strcat(path_P2, path_P2_DP(i).name),delimiterIn,
        headerlinesIn);
121             raw.P2_DP_{i} = i_P2_DP.data;
122     i_P2_DU = importdata(strcat(path_P2, path_P2_DU(i).name),delimiterIn,
        headerlinesIn);
123             raw.P2_DU_{i} = i_P2_DU.data;
124
125     i_P2_TP = importdata(strcat(path_P2, path_P2_TP(i).name),delimiterIn,
        headerlinesIn);
126             raw.P2_TP_{i} = i_P2_TP.data;
127 end
128
129 clear('path*', 'i*', '*In')
130
131
132 %-----------------------------
133 % PEAK VALUES per substrate
134 %-----------------------------
135
136 for i=1:10
137
138     peak_substrates.G(i,2) = max(raw.G_FP_{i}(:,2));
139     peak_substrates.G(i,3) = max(raw.G_FU_{i}(:,2));
140     peak_substrates.G(i,4) = max(raw.G_FO_{i}(:,2));
141     peak_substrates.G(i,5) = max(raw.G_DC_{i}(:,2));
142     peak_substrates.G(i,6) = max(raw.G_DP_{i}(:,2));
143     peak_substrates.G(i,7) = max(raw.G_DU_{i}(:,2));
144     peak_substrates.G(i,8) = max(raw.G_TP_{i}(:,2));
145
146     peak_substrates.P5(i,1) = max(raw.P5_FC_{i}(:,2));
147     peak_substrates.P5(i,2) = max(raw.P5_FP_{i}(:,2));
148     peak_substrates.P5(i,3) = max(raw.P5_FU_{i}(:,2));
149     peak_substrates.P5(i,4) = max(raw.P5_FO_{i}(:,2));
150     peak_substrates.P5(i,5) = max(raw.P5_DC_{i}(:,2));
151     peak_substrates.P5(i,6) = max(raw.P5_DP_{i}(:,2));
152     peak_substrates.P5(i,7) = max(raw.P5_DU_{i}(:,2));
153     peak_substrates.P5(i,8) = max(raw.P5_TP_{i}(:,2));
154
155     peak_substrates.P2(i,1) = max(raw.P2_FC_{i}(:,2));
156     peak_substrates.P2(i,2) = max(raw.P2_FP_{i}(:,2));
157     peak_substrates.P2(i,3) = max(raw.P2_FU_{i}(:,2));
158     peak_substrates.P2(i,4) = max(raw.P2_FO_{i}(:,2));
159     peak_substrates.P2(i,5) = max(raw.P2_DC_{i}(:,2));
160     peak_substrates.P2(i,6) = max(raw.P2_DP_{i}(:,2));
161     peak_substrates.P2(i,7) = max(raw.P2_DU_{i}(:,2));
162     peak_substrates.P2(i,8) = max(raw.P2_TP_{i}(:,2));
163 end
164
165 clear('i')
166
167
168 %-----------------------------
169 % PEAK VALUES per sample
170 %-----------------------------
171
172 peak_samples.FC = [peak_substrates.G(:,1) peak_substrates.P5(:,1) peak_substrates.
        P2(:,1)];
173 peak_samples.FP = [peak_substrates.G(:,2) peak_substrates.P5(:,2) peak_substrates.
        P2(:,2)];
```

```
peak_samples.FU = [peak_substrates.G(:,3) peak_substrates.P5(:,3) peak_substrates.
    P2(:,3)];
peak_samples.FO = [peak_substrates.G(:,4) peak_substrates.P5(:,4) peak_substrates.
    P2(:,4)];

peak_samples.DC = [peak_substrates.G(:,5) peak_substrates.P5(:,5) peak_substrates.
    P2(:,5)];
peak_samples.DP = [peak_substrates.G(:,6) peak_substrates.P5(:,6) peak_substrates.
    P2(:,6)];
peak_samples.DU = [peak_substrates.G(:,7) peak_substrates.P5(:,7) peak_substrates.
    P2(:,7)];

peak_samples.TP = [peak_substrates.G(:,8) peak_substrates.P5(:,8) peak_substrates.
    P2(:,8)];

save('data.mat', 'raw', 'peak_substrates', 'peak_samples')
```

```
%-------------------------------------------------------------------------
% CREATE BOXPLOT
%-------------------------------------------------------------------------

clear all
close all
load('data.mat')

% create vector of peak forces
x = [peak_substrates.P5(:); peak_substrates.P2(:)];
n = 10; xx = ([1:16])'; % # of rep. and samples
r = repmat(xx,1,n)';
g = r(:)';

% set positions boxes
positions = [1:16];
xpositions = [0.5:15.5];
figure('Name','PDMS')
    h=boxplot(x,g, 'positions', positions); set(h,'linewidth',1)

set(gca,'xtick',[xpositions])
set(gca,'xticklabel',{'PDMS-5: Flat Clear','PDMS-5: Flat Plain',...
        'PDMS-5: Flat UD','PDMS-5: Flat Orientation',...
        'PDMS-5: Dimple Clear','PDMS-5: Dimple Plain',...
        'PDMS-5: Dimple UD','PDMS-5: TL Plain','PDMS-2: Flat Clear',...
        'PDMS-2: Flat Plain','PDMS-2: Flat UD',...
        'PDMS-2: Flat Orientation','PDMS-2: Dimple Clear',...
        'PDMS-2: Dimple Plain','PDMS-2: Dimple UD','PDMS-2: TL Plain'},...
        'XTickLabelRotation',45)

color = ['y','b','y','c', 'm','b','y','c',...
         'y','b','y','c','m','b','y','c'];

h = findobj(gca,'Tag','Box');
for j=1:length(h)
    patch(get(h(j),'XData'),get(h(j),'YData'),color(j),'FaceAlpha',.5);
end

ax = gca; ax.YGrid = 'on';
ylabel('Peak Force [N]')

lines = findobj(gcf, 'type', 'line', 'Tag', 'Median');
set(lines, 'Color', 'r', 'LineWidth',2);
```

```
%-------------------------------------------------------------------------
% ANOVA 1
%-------------------------------------------------------------------------

clear all
close all
load('data.mat')


%-----------------------------------
% EXTERNAL STRUCTURE - Flat
%-----------------------------------

categories.int.F = {'FC' 'FP' 'FU' 'FO'};

int.F.G.value  = [  peak_samples.FP(:,1) ...
                    peak_samples.FU(:,1) peak_samples.FO(:,1)];
    [int.F.G.p, int.F.G.tbl, int.F.G.stats] = ...
                    anova1(int.F.G.value, {'FP' 'FU' 'FO'}, 'off');

int.F.P5.value  = [peak_samples.FC(:,2) peak_samples.FP(:,2) ...
                    peak_samples.FU(:,2) peak_samples.FO(:,2)];
    [int.F.P5.p, int.F.P5.tbl, int.F.P5.stats] = ...
                    anova1(int.F.P5.value, categories.int.F, 'off');

int.F.P2.value  = [peak_samples.FC(:,3) peak_samples.FP(:,3) ...
                    peak_samples.FU(:,3) peak_samples.FO(:,3)];
    [int.F.P2.p, int.F.P2.tbl, int.F.P2.stats] = ...
                    anova1(int.F.P2.value, categories.int.F, 'off');


    % ----------------------------------------
    % multicomparison flat - FC, FP, FU, FO
    % ----------------------------------------
    [int.F.G.c,~,~,~] = multcompare(int.F.G.stats);
    [int.F.P5.c,~,~,~] = multcompare(int.F.P5.stats);
    [int.F.P2.c,~,~,~] = multcompare(int.F.P2.stats);


%-----------------------------------
% EXTERNAL STRUCTURE - Dimples
%-----------------------------------

categories.int.D = {'DC' 'DP' 'DU'};
int.D.G.value  = [peak_samples.DC(:,1) peak_samples.DP(:,1) peak_samples.DU(:,1)];
    [int.D.G.p, int.D.G.tbl, int.D.G.stats] = ...
                    anova1(int.D.G.value, categories.int.D, 'off');

int.D.P5.value  = [peak_samples.DC(:,2) peak_samples.DP(:,2) peak_samples.DU(:,2)];
    [int.D.P5.p, int.D.P5.tbl, int.D.P5.stats] = ...
                    anova1(int.D.P5.value, categories.int.D, 'off');

int.D.P2.value  = [peak_samples.DC(:,3) peak_samples.DP(:,3) peak_samples.DU(:,3)];
    [int.D.P2.p, int.D.P2.tbl, int.D.P2.stats] = ...
                    anova1(int.D.P2.value, categories.int.D, 'off');


    % ----------------------------------------
    % multicomparison dimples - DC, DP, DU
    % ----------------------------------------

    [int.D.G.c,~,~,~] = multcompare(int.D.G.stats);
    [int.D.P5.c,~,~,~] = multcompare(int.D.P5.stats);
    [int.D.P2.c,~,~,~] = multcompare(int.D.P2.stats);


```

```
67 %-----------------------------------
68 % INTERNAL STRUCTURE - Clear
69 %-----------------------------------
70
71 categories.ext.C = {'FC'; 'DC'};
72
73 ext.C.P5.value = [peak_samples.FC(:,2) peak_samples.DC(:,2)];
74     [ext.C.P5.p, ext.C.P5.tbl, ext.C.P5.stats] = ...
75                     anova1(ext.C.P5.value, categories.ext.C, 'off');
76
77 ext.C.P2.value = [peak_samples.FC(:,3) peak_samples.DC(:,3)];
78     [ext.C.P2.p, ext.C.P2.tbl, ext.C.P2.stats] = ...
79                     anova1(ext.C.P2.value, categories.ext.C, 'off');
80
81
82 %-----------------------------------
83 % INTERNAL STRUCTURE - Plain
84 %-----------------------------------
85
86 categories.ext.P = {'FP'; 'DP'; 'TP'};
87
88 ext.P.G.value  = [peak_samples.FP(:,1) peak_samples.DP(:,1) peak_samples.TP(:,1)];
89     [ext.P.G.p, ext.P.G.tbl, ext.P.G.stats] = ...
90                     anova1(ext.P.G.value, categories.ext.P, 'off');
91
92 ext.P.P5.value = [peak_samples.FP(:,2) peak_samples.DP(:,2) peak_samples.TP(:,2)];
93     [ext.P.P5.p, ext.P.P5.tbl, ext.P.P5.stats] = ...
94                     anova1(ext.P.P5.value, categories.ext.P, 'off');
95
96 ext.P.P2.value = [peak_samples.FP(:,3) peak_samples.DP(:,3) peak_samples.TP(:,3)];
97     [ext.P.P2.p, ext.P.P2.tbl, ext.P.P2.stats] = ...
98                     anova1(ext.P.P2.value, categories.ext.P, 'off');
99
100
101     % ---------------------------------------
102     % multicomparison plain - FP, DP, TP
103     % ---------------------------------------
104
105     [ext.P.G.c, ext.P.G.m, ext.P.G.h, categories.ext.P] = ...
106         multcompare(ext.P.G.stats);
107
108     [ext.P.P5.c, ext.P.P5.m, ext.P.P5.h, categories.ext.P] = ...
109         multcompare(ext.P.P5.stats);
110
111     [ext.P.P2.c, ext.P.P2.m, ext.P.P2.h, categories.ext.P] = ...
112         multcompare(ext.P.P2.stats);
113
114
115 %-----------------------------------
116 % INTERNAL STRUCTURE - UD
117 %-----------------------------------
118
119 categories.ext.U = {'FU'; 'DU'};
120
121 ext.U.G.value  = [peak_samples.FU(:,1) peak_samples.DU(:,1)];
122     [ext.U.G.p, ext.U.G.tbl, ext.U.G.stats] = ...
123                     anova1(ext.U.G.value, categories.ext.U, 'off');
124
125 ext.U.P5.value = [peak_samples.FU(:,2) peak_samples.DU(:,2)];
126     [ext.U.P5.p, ext.U.P5.tbl, ext.U.P5.stats] = ...
127                     anova1(ext.U.P5.value, categories.ext.U, 'off');
128
129 ext.U.P2.value = [peak_samples.FU(:,3) peak_samples.DU(:,3)];
130     [ext.U.P2.p, ext.U.P2.tbl, ext.U.P2.stats] = ...
131                     anova1(ext.U.P2.value, categories.ext.U, 'off');
132
133
```

```
%-----------------------------------
% SUBSTRATES
%-----------------------------------

categories.sub = {'G' 'P5' 'P2'};

[sub.FC.p, sub.FC.tbl, sub.FC.stats] = ...
                anova1([peak_samples.FC(:,2) peak_samples.FC(:,3)],...
                                                {'P5' 'P2'}, 'off');

[sub.FP.p, sub.FP.tbl, sub.FP.stats] = ...
                anova1(peak_samples.FP, categories.sub, 'off');

[sub.FU.p, sub.FU.tbl, sub.FU.stats] = ...
                anova1(peak_samples.FU, categories.sub, 'off');

[sub.FO.p, sub.FO.tbl, sub.FO.stats] = ...
                anova1(peak_samples.FO, categories.sub, 'off');


[sub.DC.p, sub.DC.tbl, sub.DC.stats] = ...
                anova1(peak_samples.DC, categories.sub, 'off');

[sub.DP.p, sub.DP.tbl, sub.DP.stats] = ...
                anova1(peak_samples.DP, categories.sub, 'off');

[sub.DU.p, sub.DU.tbl, sub.DU.stats] = ...
                anova1(peak_samples.DU, categories.sub, 'off');

[sub.TP.p, sub.TP.tbl, sub.TP.stats] = ...
                anova1(peak_samples.TP, categories.sub, 'off');


    % ---------------------------------------
    % multicomparison - all except FC, DC
    % ---------------------------------------
    [sub.FP.c,~,~,~] = multcompare(sub.FP.stats);
    [sub.FU.c,~,~,~] = multcompare(sub.FU.stats);
    [sub.FO.c,~,~,~] = multcompare(sub.FO.stats);

    [sub.DC.c,~,~,~] = multcompare(sub.DC.stats);
    [sub.DP.c,~,~,~] = multcompare(sub.DP.stats);
    [sub.DU.c,~,~,~] = multcompare(sub.DU.stats);
    [sub.TP.c,~,~,~] = multcompare(sub.TP.stats);
```

```
%-------------------------------------------------------------------------
% ANOVA 2
%-------------------------------------------------------------------------

clear all
close all
load('data.mat')


%---------------------
% Groups & y-values
%---------------------

    % group sequence for 1 measurement on all substrates
    g.seq.ext = {'F' 'F' 'F' 'F' 'D' 'D' 'D' 'T' ...
                 'F' 'F' 'F' 'F' 'D' 'D' 'D' 'T'};

    g.seq.int = {'C' 'P' 'U' 'O' 'C' 'P' 'U' 'P' ...
                 'C' 'P' 'U' 'O' 'C' 'P' 'U' 'P'};
```

```
20
21      g.seq.sub = {    'P5' 'P5' 'P5' 'P5' 'P5' 'P5' 'P5' 'P5' ...
22                       'P2' 'P2' 'P2' 'P2' 'P2' 'P2' 'P2' 'P2'};
23
24      % group for 10 consequetive measurements
25      for i=10:10:160
26          for j = 0:9
27              g.ext_sub{1}{(i-j),1} = g.seq.ext{i/10};
28              g.ext_sub{2}{(i-j),1} = g.seq.sub{i/10};
29
30              g.int_sub{1}{(i-j),1} = g.seq.int{i/10};
31              g.int_sub{2}{(i-j),1} = g.seq.sub{i/10};
32          end
33      end
34      clear('i','j');
35
36  y = [peak_substrates.P5(:); peak_substrates.P2(:)];
37
38
39  %-----------------------------------
40  % ANOVA2 - ext*sub and int*sub
41  %-----------------------------------
42
43  [ext_sub.p, ext_sub.tbl, ext_sub.stats]  = anovan(y, g.ext_sub,...
44                           'model',2,'varnames',{'ext','sub'});
45
46  [int_sub.p, int_sub.tbl, int_sub.stats]  = anovan(y, g.int_sub,...
47                           'model',2,'varnames',{'int','sub'});
48
49
50      %-----------------------
51      % Multicomparison
52      %-----------------------
53
54      [ext_sub.mult.ext.c,~,~,~] = multcompare(ext_sub.stats,'Dimension',1);
55      [ext_sub.mult.sub.c,~,~,~] = multcompare(ext_sub.stats,'Dimension',2);
56      [ext_sub.mult.c,~,~,~] = multcompare(ext_sub.stats,'Dimension',[1,2]);
57
58      [int_sub.mult.int.c,~,~,~] = multcompare(int_sub.stats,'Dimension',1);
59      [int_sub.mult.sub.c,~,~,~] = multcompare(int_sub.stats,'Dimension',2);
60      [int_sub.mult.c,~,~,~] = multcompare(int_sub.stats,'Dimension',[1,2]);
```